

Lagrangian-based trajectory modelling of the Hunga Tonga-Hunga Ha’apai (HTHH) Eruption in ABL using meteorological data from mid-week of January 2022

Sarbojeet Bhowmick^{1,2}, David Sládek³, Josef Vojtěch¹, Lada Altmannová¹, and Radek Velc¹

¹Department of Optical Networks, CESNET, Prague, Czech Republic

²Faculty of Environmental Sciences, Czech University of Life Sciences Prague, Czech Republic

³Faculty of Military Technology, University of Defence, Brno, Czech Republic

July 23, 2023

Key Points:

- Lagrangian-based HYSPLIT modelling system used to estimate volcanic ash particle trajectories.
- HYSPLIT simulation took place before and after the massive eruption on 15th January 2022 (termed as pre-caldera and post-caldera respectively in Section 5)
- Volcanic ash particle deposition and volcanic ash particle position simulated using HYSPLIT for the HTHH submarine volcano massive eruption event.

Abstract

Volcano-seismic signals such as long-period (LP) events and tremors are important indicators for volcanic activity and unrest. Explosive volcanic eruptions are stunning phenomena that influence the Earth’s natural systems and climate in a variety of ways. This paper discusses the mid-week January 2022 eruption of the HTHH submarine volcano, especially on 15th January an event with many impacts in the region (dynamic, chemical, climate breakdown). Given the potential for a volcanic eruption to affect climate, the oceanic system, or climate variability, consistent and understandable modelling of these exceptional events is critical.

The main objective was to determine the volcanic effects in our atmospheric boundary layer (ABL) during the multiple eruptive events occurred on January 2022 at HTHH. Our discussion also contributes to understanding the underlying Earth system dynamics triggered by cataclysmic volcanic eruptions. The Hybrid Single-Particle Lagrangian Integrated Trajectory (HYSPLIT) model system developed by the National Oceanic and Atmospheric Administration’s (NOAA) Air Resources Laboratory was used to deliberate the effects caused by the multiple eruptions of HTHH on mid-week of January 2022. Our modelling results include model trajectories at different frequency levels, volcanic ash deposition and ash particle position from the series of multiple eruption events of submarine volcano HTHH in the mid-week of January 2022.

Plain Language Summary

The submarine volcano HTHH had a significant impact on volcano-seismic activity over an extended period of time. The volcanic activity and resulting unrest had diverse effects on Earth’s climate and other crucial natural processes. Seismic events from multiple eruptions influenced dynamic activity, chemical composition, and ultimately led to climate changes. The potential of submarine volcano eruptions to disturb the oceanic system, affect climate, and induce climate variability is exceptional. It is crucial to develop consistent and

specialized analytical models to understand the hidden effects of multiple HTHH events on the Earth's system. In our study, we analysed the outcomes using the HYSPLIT modelling system in the Atmospheric Boundary Layer (ABL), which was activated by explosive tremor events in HTHH. The use of HYSPLIT by NOAA facilitated the modelling of the effects of multiple explosive eruptions of HTHH during that period. The results encompassed trajectories at various altitudes, volcanic ash deposition, and the positioning of volcanic ash particles. For future planning of volcanic explosive events and understanding their climatic aftermath, the modelling results from this study can offer valuable insights in the HTHH volcanic region.

1. Introduction

The submarine volcano HTHH experienced multiple eruptions, which are often accompanied by various seismo-volcanic signals, including very long-period (VLP) events, long-period (LP) events, volcano-tectonic (VT) events, and tremor. These signals provide valuable information about the physical processes occurring at depth and are used to assess the activity state of a volcano. Monitoring observatories continuously analyse these events, considering factors such as their number, amplitude, location, and temporal variations, for early warning purposes.

Each type of volcano-seismic event has distinct characteristics and underlying processes. VT earthquakes exhibit a broad frequency content between 2 and 20 Hz and have an impulsive onset, like tectonic earthquakes. LP events occur in a narrow frequency band of 0.5 to 5 Hz, with a dominant frequency content between 0.5 and 2 Hz. The source process of LP events is still a topic of debate. VLP events share waveform similarities with LP events but have frequencies ranging from 0.01 to 0.5 Hz. Tremor is a long-lasting, emergent seismic signal that can exhibit a broad or harmonic frequency content, showing spectral characteristics like LP events.

Volcano observatories employ seismic sensor networks or arrays to detect and locate these transient and continuous signals. VT events are located using P and/or S wave arrival times, while LP events are located using polarization analysis, P-wave picking, waveform similarity-based methods, or amplitude decay analysis. Tremor is located based on seismic amplitude decrease or phase shifts within a network or seismic array. Conventional seismic monitoring on volcanoes typically involves networks equipped with translational sensors, while portable rotational sensors record ground rotation rates around three axes.

The Lagrangian Transport Model (LTM) used in this study employs Lagrangian calculations based on a reference frame that moves with the river flow. This approach avoids the need for numerical calculation of the convective component of the convection-diffusion equation. In this paper, we utilized HYSPLIT as an LTM to generate backward air mass trajectories up to a specific height, which is crucial for simulating pollution transport. Specifically, HYSPLIT 4 was employed as an LTM to simulate the transport and dispersion of volcanic ash and gases during the studied event.

LTMs have been widely used in research, including studies on volcanic sulphur dioxide (SO₂) emissions. Researchers have utilized HYSPLIT to model the transport and dispersion of volcanic SO₂ from different volcanoes. Their simulations showed good agreement with satellite measurements, highlighting the effectiveness of Lagrangian-based trajectory modelling in predicting volcanic SO₂ injections.

Lagrangian-based trajectory modelling, such as the HYSPLIT model, offers valuable advantages for calculating the injection and dispersion of volcanic gases and particles. Numerous case studies have demonstrated its effectiveness in enhancing our understanding of the environmental and climatic impacts of volcanic eruptions. Compared to other models, Lagrangian-based HYSPLIT modelling provides several benefits that are specific to the scientific application.

One key advantage is the ability to achieve a high level of physical realism. Lagrangian models can capture sub-grid scale information that may be missed by other models. This allows for a more detailed representation of the processes involved in gas and particle transport during volcanic eruptions. Additionally, Lagrangian models exhibit numerical stability, meaning they introduce less artificial diffusion compared to Eulerian-based models.

HYSPLIT, like other conservation models, ensures mass and energy conservation throughout the simulation. This is crucial for accurately representing the physical behaviour of volcanic emissions. Furthermore, HYSPLIT demonstrates computational efficiency and can easily handle complex geometries, making it suitable for studying air deposition and trajectory levels. Its ability to accurately track particle movement in the atmosphere contributes to its usefulness in analysing volcanic ash dispersion, as demonstrated in this study.

2. Composition of the ash particle trajectories

This paper focus on the volcanic ash particle trajectory at different frequency levels for multiple eruptions that occurred at the submarine volcano HTHH specifically mid-week of January 2022 (14th-18th January 2022). The magnitude spectrum equation in the frequency domain is computed using $\text{abs}(X_f)$ from the complex output X_f . In contrast, the phase spectrum is derived using $\text{angle}(X_f)$ and indicates the phase shift of each frequency component of a signal. Using Fourier transform, the obtained signal converted from the time domain to the frequency domain, where it could be expressed as a complex frequency function. The amplitude of that component is the modulus of this complex function, and its argument is the relative phase shift of that wave. In addition to being easier to solve algebraically, seeing a system via the lens of frequency may frequently provide an intuitive insight of its qualitative behaviour. The magnitude spectrum equation is used to determine the relative intensity of frequency components in a signal. The magnitude spectrum is calculated by multiplying the magnitude of the analytic signal by its phase angle. The magnitude spectrum is shown by a plot of $|X(w)|$ versus w , where $X(w)$ is the Fourier transform of the signal $x(t)$.

The HYSPLIT model system is essentially based on Lagrangian dispersion models, which offered descriptive predictions for air pollution distribution in both homogeneous and inhomogeneous turbulent airflows. The Lagrangian dispersion model, which is based on a simulation of tracer trajectories, naturally describes pollutant transport and is numerically simple. Based on Thomson (1987) the Lagrangian model unfolds the characteristics on the movement of a passive particle in a turbulent flow which can be adequately described by a nonlinear stochastic equation system as follows:

$$dU_i = a_i dt + b_{ij} d\xi_j$$

$$dX_i = U_i dt$$

.... Equation 1 (Yaping Shao, 1991)

Here, U_i and X_i are the velocity and position of the particle, respectively; t is time; and $d\xi_j$ is a random acceleration. The coefficients a_i and b_{ij} are determined by the structure of turbulence. Using this method, a complete understanding of atmospheric turbulence over uniform surfaces has been achieved and this has provided a solid basis for the application of Lagrangian models. In this paper, volcanic ash particle trajectories (See in Section 4) have been obtained using HYSPLIT.

Lagrangian models of tracer-particle trajectories in turbulent flows can be adapted for simulation of particle trajectories. This is conventionally done by replacing the zero mean fall speed of a tracer-particle with the terminal speed of the particle. Such models have been used widely to predict spore and pollen dispersal (Andy M. Reynolds et al., 2018). In ABL, Pope (2000) proposed that intermittency in ϵ can play a significant role, where the ratio between ϵ and its time-averaged value ($\overline{\epsilon}$) can reach as high as 50. However, in Lagrangian stochastic (LS) particle trajectory models have significant impact on the intermittent behaviour of ϵ . Thomson (1987); Wilson and Sawford (1996) studies show that LS models typically do not consider for the intermittent behaviour of ϵ . LS models estimate a local Lagrangian time scale as a function of a local ϵ . Studies from Pope and Chen (1990) using an extended LS model that includes not only the instantaneous velocity, but also the instantaneous dissipation (ϵ) along a particle trajectory. In this model, where the dissipation rate ϵ is sampled from a log-normal probability density function (PDF), by solving an additional stochastic differential equation for $\chi = \ln(\epsilon/\overline{\epsilon})$.

T. Haszpra and T. Tél (2011) discovered that the Maxey-Riley equations yield the equations of motion for tiny, inertial, spherical particles of radius r in a viscous fluid advected by a flow deterministically (M. Farazmand and G. Haller, 2014). The dimensionless equations for the particles trajectory $r_p(t)$ for heavy particles with density p significantly greater than that of the ambient medium are as follows:

$$\ddot{r}_p = 1/St \cdot (\dot{v}(r,t) - \dot{r}_p) - W_{\text{terminal}} n$$

.... Equation 2 (T. Haszpra and T.

Tél, 2011)

where $v(r, t)$ is the flow field, W_{terminal} is the dimensionless terminal velocity in still fluid, and n is an upward-pointing unit vector. The units of velocity and distance are characteristic velocity units, U and L , respectively. The dimensionless relaxation period of inertial particles exposed to Stokes drag is denoted by the Stokes number (St). Typically, the limit of $St \rightarrow 0$ in (equation 2) indicates finite acceleration only if the parenthesis on the right-hand side disappears, and the large-scale equation of motion for aerosol particles becomes even simpler than before. On the contrary, the inertial effects are minor, but deposition must be considered with a terminal velocity in the vertical direction.

In this paper, we used magnitude spectrum to get the relative intensity of the BH1 frequency channel from HTHH eruption event on 15th January 2022 at 4:12 UTC can be seen in Fig. 1. For charting vibration spectra, logarithmic amplitude scaling is preferable to linear amplitude scaling because it allows for better evaluation of extremely tiny components in a spectrum. Linear amplitude scaling makes the larger components of a spectrum highly visible and easy to analyse, but it might make very small components impossible to perceive. The technique of spectral balancing is used to flatten the frequency content and amplitude spectra of seismic data. This approach can increase vertical resolution in seismic amplitude volumes by revealing narrow channels and visible edges. Following spectral balancing, energy ratio coherence can be applied to both the input data and the spectrally balanced data. Spectral decomposition may also be used to spectrally balanced versions of raw seismic data, allowing equal time slices to be computed from speech component volumes.

To summarise, spectral magnitude is an energy measurement that corresponds with the trace in seismic data. The seismic moment and magnitude can be estimated via spectral analysis as shown in Fig. 1.

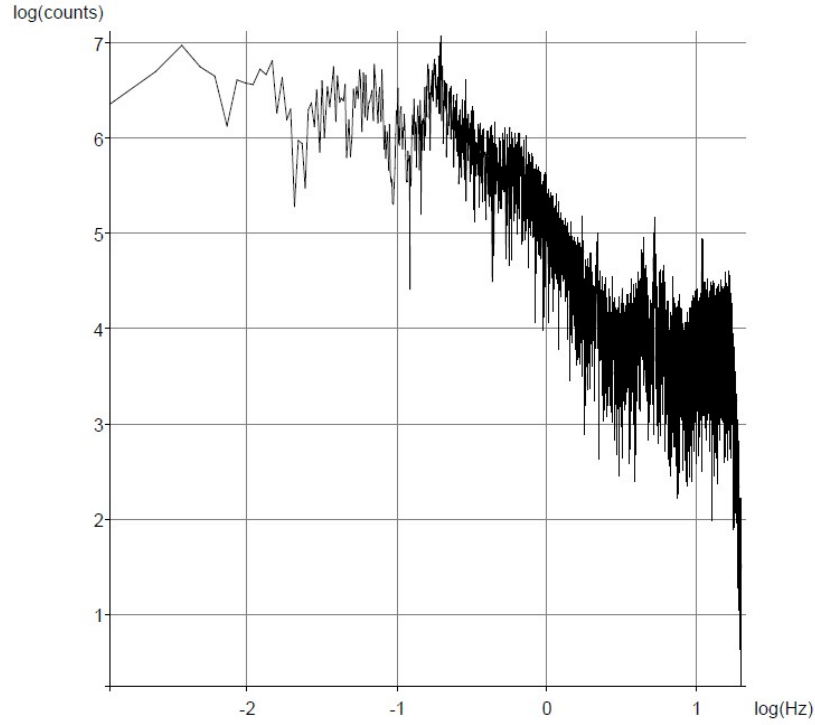


Figure 1: Spectral magnitude graph from the HTHH massive eruption that occurred on 15th January 2022 at 4:12 hrs (UTC)

A seismogram's frequency content may be viewed as it varies over time using a spectrogram. Spectral balancing is a method used in seismic data to flatten the frequency content and amplitude spectra, enhancing vertical resolution, and displaying narrow channels and distinct edges.

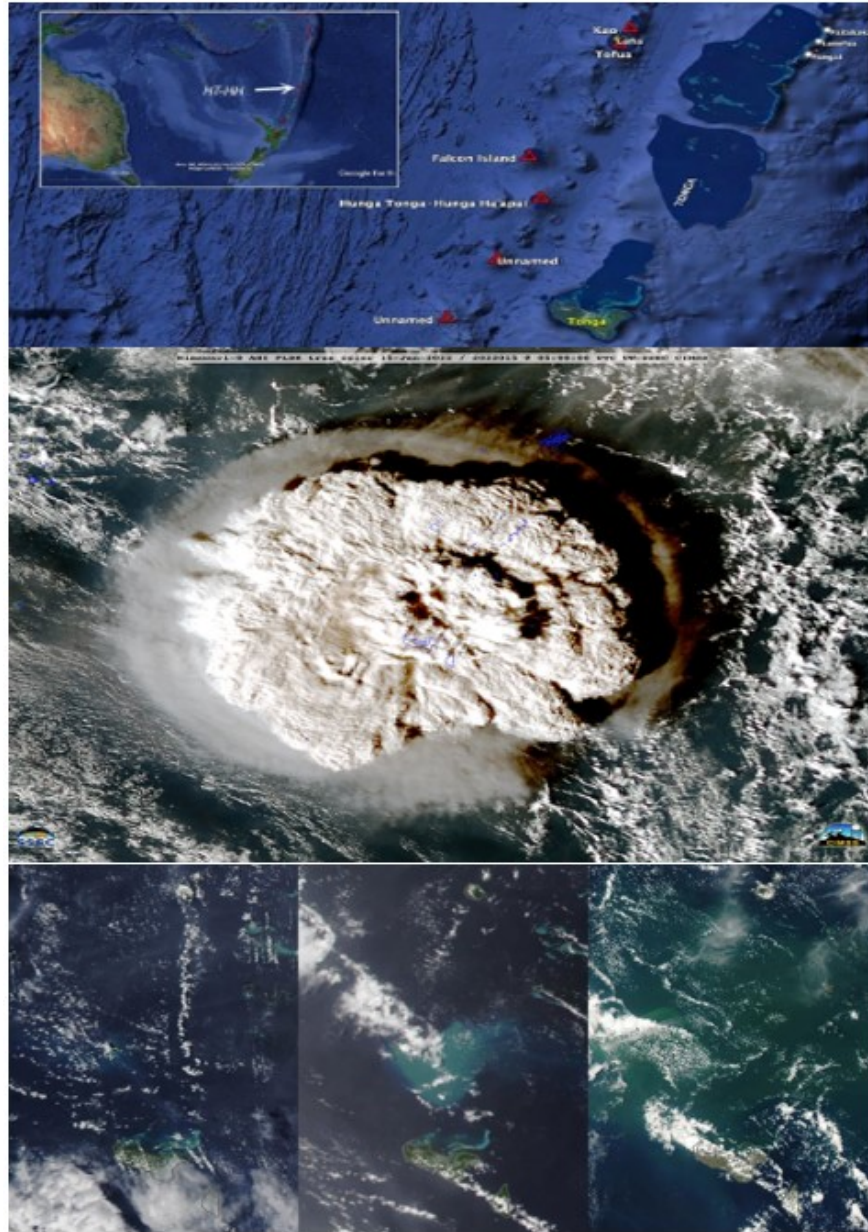


Figure 2: Shows the GOES-17 satellite image of the HTHH Eruption that happened on 15th January 2022. Below three images from left to right are satellite images taken later the massive eruption event on 15th January 2022

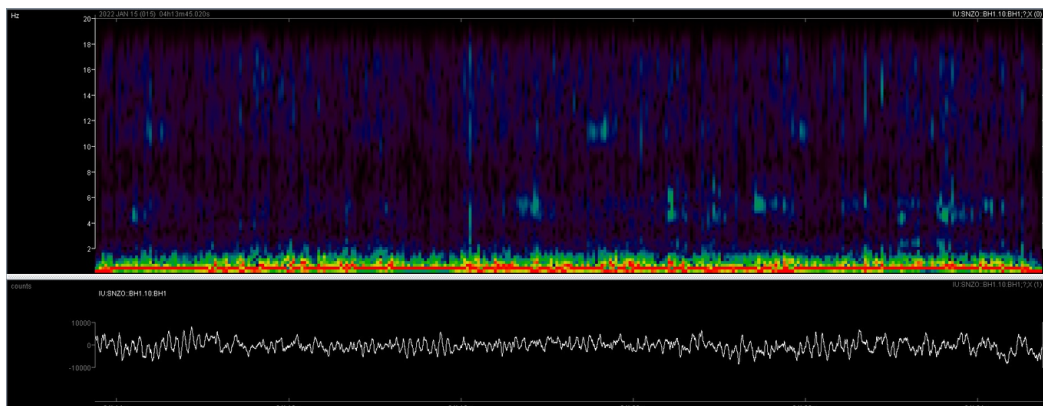


Figure 3: Shows the spectrogram from the caldera submarine HTHH volcano eruption that occurred on 15th January 2022 at 4:12 hrs (UTC) using the BH1 channel data (Data obtained from PyWEED software)

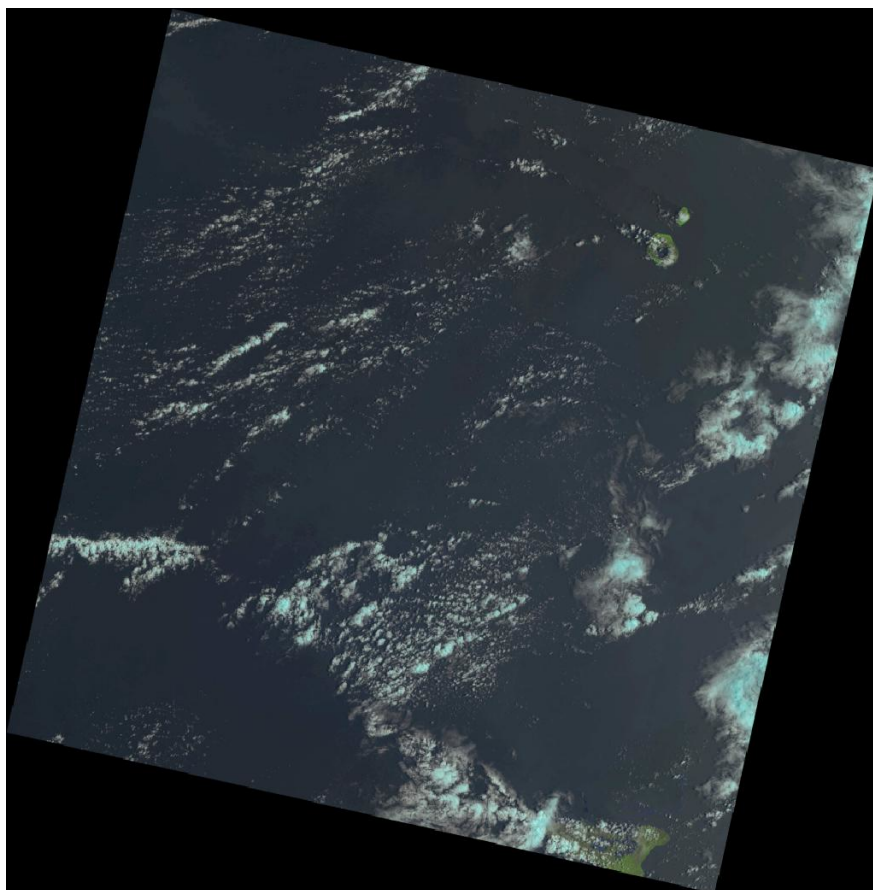
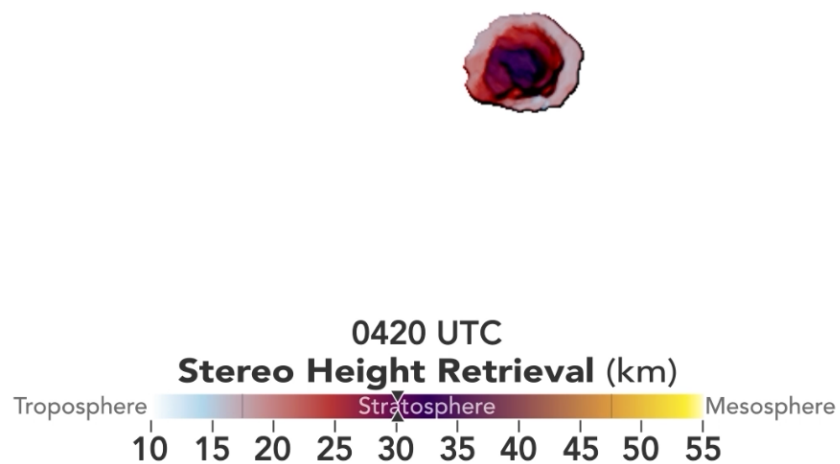


Figure 4: Image collected from the LANDSAT 8-9 (Level 2) monitored on January 17, 2022 after the massive eruption of submarine volcano HTHH

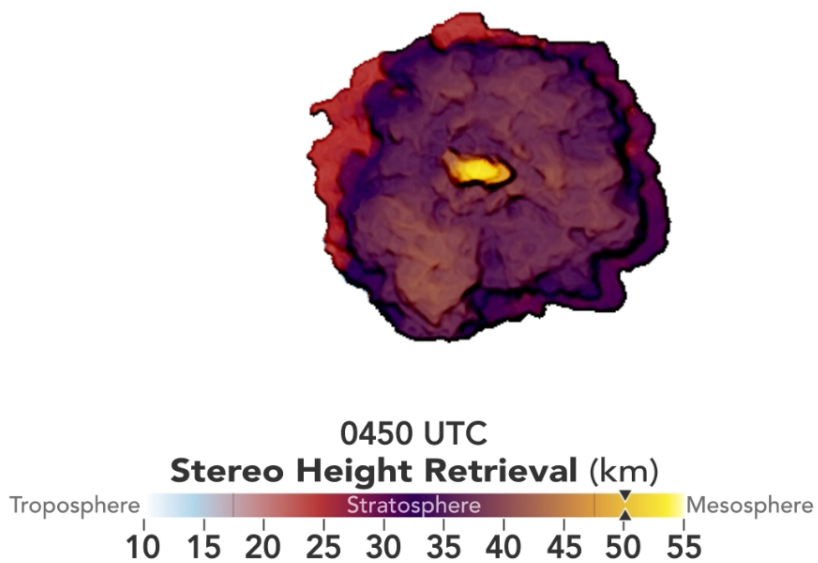
2.1 Volcanic ash cloud transport

Submarine eruptions are volcanic eruptions that occur underneath the water’s surface. Due to hotspots, these eruptions can occur near constructive edges, subduction zones, and within tectonic plates. Throughout geological history, explosive submarine eruptions have occurred in a variety of submarine environments. The accompanying deposits indicate that the eruption of fractured magma-seawater mixes forms ascending flows that eventually feed an undersea flow and fall deposits. Deposits from explosive submarine eruptions have been reported 1-4 km below the surface in the deep sea, with both flow and fall deposits ranging several kilometres over the seafloor. However, there is no precise information about “submarine volcano cloud transport” available. Yet, based on known data on undersea eruptions using HYSPLIT models, it can be concluded that volcanic ash is transported through water during a submerged eruption in the same way as it is transported through air during an aerial eruption. The difference would be that it would be transported through water rather than the atmosphere.

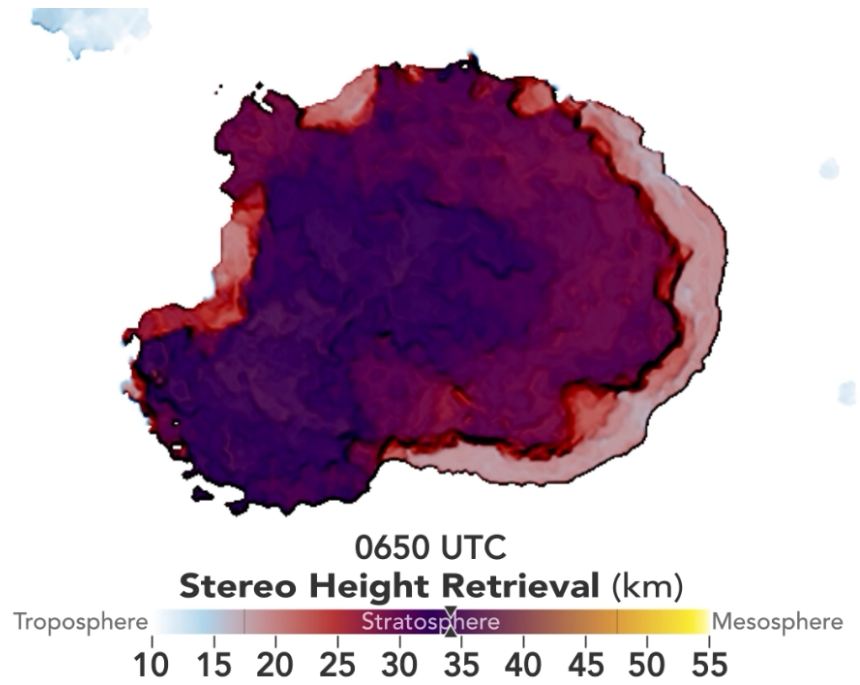
In the atmospheric sciences field, the HYSPLIT model is a frequently used atmospheric transport and dispersion model. The model replicates the dispersion and trajectory of chemicals carried and diffused through our atmosphere on local to global dimensions. It is intended to facilitate a wide variety of simulations concerning the movement and dispersion of pollutants and dangerous compounds in the atmosphere. Data acquisition delay varies depending on the sensor and method utilized for real-time monitoring of volcanic ash clouds. The NOAA/CIMSS Volcanic Cloud Monitoring website, for example, provides near-real-time processing of multiple geostationary and low-Earth orbit satellites that cover a large portion of the globe. The delay period for using CATS near-real-time lidar measurements to monitor volcanic ash clouds is around 3-6 hours. The use of DB/DR data processing might eventually lower the temporal lag for day-night monitoring of volcanic SO₂ and ash clouds. Nevertheless, there is no universal number for data acquisition latency because it is affected by several aspects such as the type of sensor, technique, and processing involved. The utilisation of GEO satellite data is necessary for the early identification and tracking of volcanic ash plumes and cloud movements. Volcanic eruptions may now be predicted using thermal infrared remote sensing technologies. Nevertheless, there is no information on the typical latency time for monitoring volcanic ash clouds utilizing GEO satellite data or thermal infrared remote sensing technologies. Early detection and tracking of volcanic ash plumes and cloud trajectories requires the use of GEO satellite data. The principal observables of volcanoes include deformation, surface alteration, gas emissions, temperature anomalies, and ash clouds. Deformation has been proven to precede volcanic eruptions in terms of predicting. Because of high-temporal-resolution geostationary and polar-orbiting meteorological satellite data, gas emissions and thermal anomalies may be detected in near-real time. Yet, because of their fluctuating composition and size dispersion, ash clouds are more difficult to observe. Even with a lag of one hour owing to propagation time, worldwide infrared monitoring can offer timely information to Volcanic Ash Advisory Centres (VAAC). Observational data from satellite remote sensing networks are crucial in estimating the ash cloud’s 4D dispersion. In this paper, we use HYSPLIT modelling system to monitor the ash cloud trajectories during the event. To summarize, several factors influence the latency time for monitoring volcanic ash clouds. They include satellite data difficulties such as delay and limited access to pictures. Mesoscale scanning can greatly reduce latency, while distant sensing networks play an important role in identifying the 4D dispersion of the ash cloud.



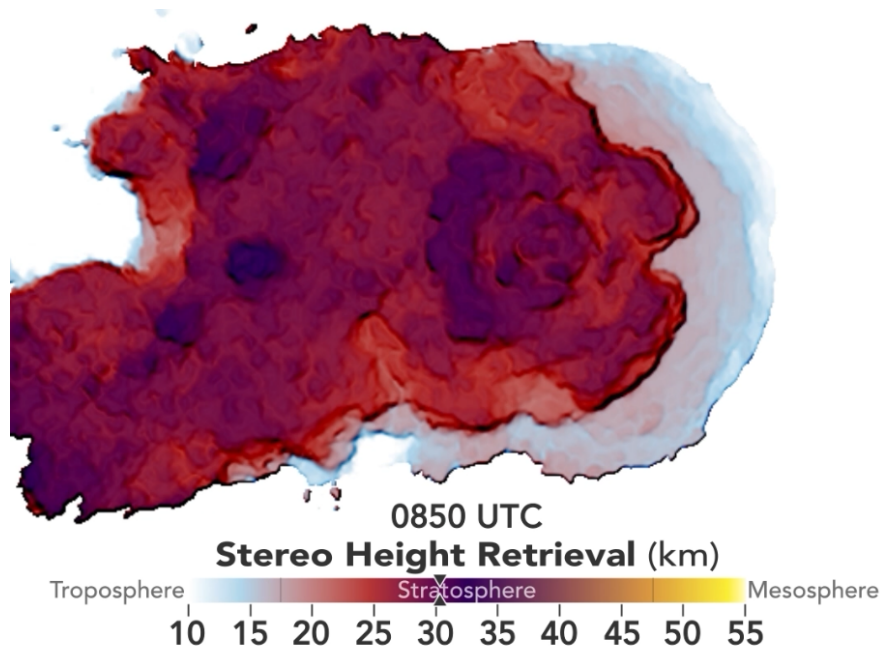
[a]



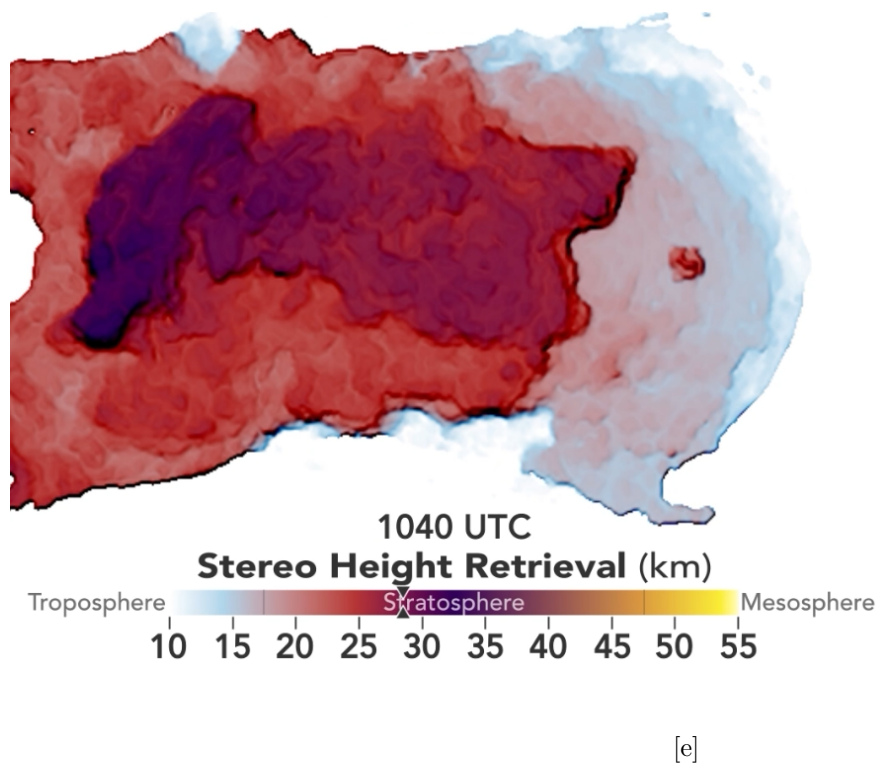
[b]



[c]



[d]



Below [f]

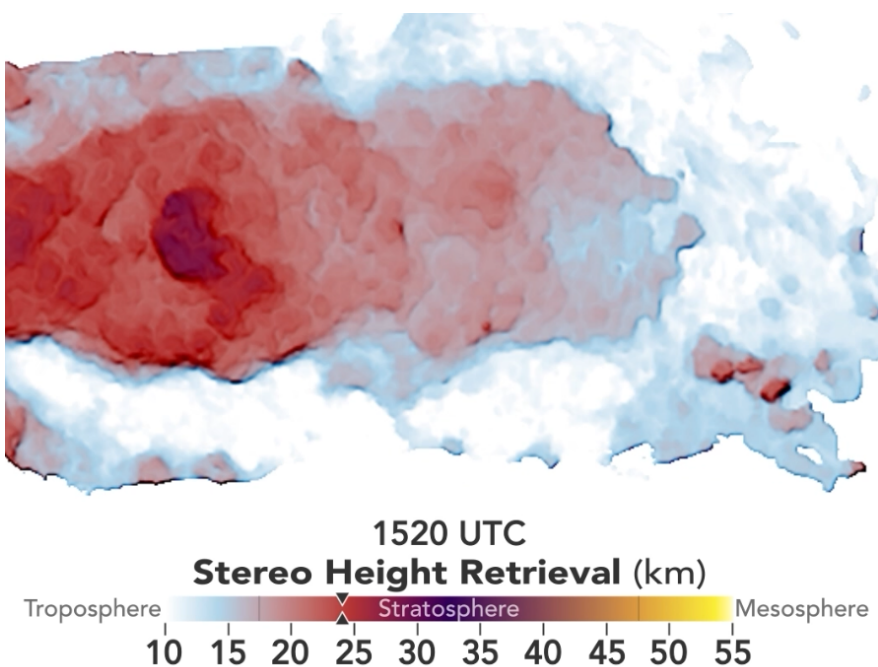


Figure 5: Figures (a-f), describes the volcanic ash cloud transport in ABL on 15th January 2022 from HTHH submarine volcano eruption since the beginning of event time at 4:20 UTC and throughout the day till 15:20 UTC at different timestamps.

2.2 Volcanic ash cloud composition

The rock, mineral, and glass particles that make up volcanic ash are expelled by a volcano during an eruption. The particles are under 2 mm in diameter. Rock shards, mineral crystals, and volcanic glass all make up volcanic ash. The composition of volcanic ash is determined by the chemistry of the magma from which it generally formed. It has not been established that most of the minerals found in ash are harmful to human health. Volcanic ash's chemical makeup changes according to the kind of volcano and the minerals contained in the magma. In general, from a stratovolcano volcano, volcanic ash is composed of roughly 65% SiO₂, 18% Al₂O₃, 5% Fe₂O₃, 2% MgO, 4% CaO, 4% Na₂O, and 0.1% S. In addition to these primary components, 37 trace metals have been identified, including Ba, Cu, Mn, Sr, V, Zn, and Zr. Volcanic ash contains fundamental minerals such as quartz and tridymite, as well as secondary minerals such as kaolin-group minerals and alunite. Volcanic ash's physical and chemical characteristics are largely influenced by the eruption style. Basaltic air-borne pyroclastic materials have a silica content ranging from 45 to 53.5%, intermediate (andesitic) air-borne pyroclastic materials have a silica content ranging from 53.5 to 62%, and felsic (dacitic and rhyolitic) air-borne pyroclastic materials have a silica content of greater than 62%.

In case of submarine volcanoes, they dump massive amounts of stuff into the oceans, including ash. Volcanic ash has long been detected in marine sediment, and its chemical composition can be utilized to estimate the chemical composition of undersea volcanic ash. One strategy is to quantify distributed volcanic ash in marine sand using geochemical methods. Another method is to use the chemical makeup of volcanic ash deposits to determine their origin.

Scientists developed a relationship between the color and chemical content of discoloured seawater in the vicinity of an underwater volcano. This approach, however, may not be suitable for identifying the chemical composition of undersea volcanic ash. Microbial communities found in sediments differ greatly from those found in hydrothermal fluids. Volcanic ash, such as that seen in the Kermadec arc, is a kind of sediment formed by explosive eruptions. Scientists evaluated microbial community compositions and functioning in two hydrothermal fluid and one tephra (volcanic ash deposit) samples taken from the Kermadec arc in research published in *Frontiers in Microbiology*. The study discovered that characteristics influencing community structure and element cycling have a significant influence on local element cycling, such as sulphur and nitrogen cycling, Fe-S-mineral precipitation, and the employment of iron (III) as an electron acceptor. Generally, knowing the chemical composition of undersea volcanic ash necessitates the use of geochemical approaches or pinpointing its origins through chemical composition.

2.3 Volcanic ash particle monitoring

For the purpose of identifying and tracking volcanic eruptions and ash in the atmosphere, satellite sensors are crucial. The Advanced Baseline Imager (ABI) on GOES-16 and GOES-17 is the principal surveillance instrument for volcanic clouds. VAAC forecasters utilize ABI data to track clouds whose position, evolution, and/or spectral features correspond to volcanic activity. Volcanic ash detection and monitoring are crucial for ensuring safety and reducing economic damage. The height of a volcanic cloud indicates the severity of an explosive event. Flight level (FL) represents the top of a laterally expanding volcanic cloud and is used to report volcanic cloud height. Researchers examine the average volcanic ash cloud height per occurrence in comparison to that allocated by the M-ESP database to determine how the activity recorded within Volcanic Ash Advisory Areas (VAAs) relates to predicted activity for a specific volcano.

In addition to satellite sensors, a strategy for increased detection of airborne volcanic ash has been developed based on visible (VIS), near-infrared (NIR), shortwave infrared (SWIR), mid-wave infrared (MWIR), long-wave infrared (LWIR), ultraviolet (UV), microwave radiometry, lidar, radar, or combinations thereof. Remote sensing technology is used by satellite sensors to detect volcanic ash. For nearly 20 years, the split window or reverse absorption approach has been employed. The brightness temperatures recorded using two distinct wavelengths of infrared light, which react differently when they travel through clouds of volcanic ash or water droplets, are compared in this approach. Volcanic cloud monitoring is frequently done using the SEVIRI

sensor on Meteosat Second Generation (MSG) geostationary satellites. It has a spatial resolution of 3 km at the equator and 4.5 km in Mediterranean latitudes, and it measures radiances in 12 spectral channels spanning the visible to infrared spectrums. Thermal infrared remote sensing can identify volcanic ash clouds fast and precisely. Unfortunately, the inter-band correlations in remote sensing data are rather significant, making it difficult to discern between different types of land cover and atmospheric conditions. Researchers have created algorithms that employ numerous sensors, including lidar and radar data, as well as thermal infrared data from satellites, to improve the accuracy of airborne volcanic ash detection. These algorithms can offer more precise data on the position, height, and concentration of volcanic ash clouds.

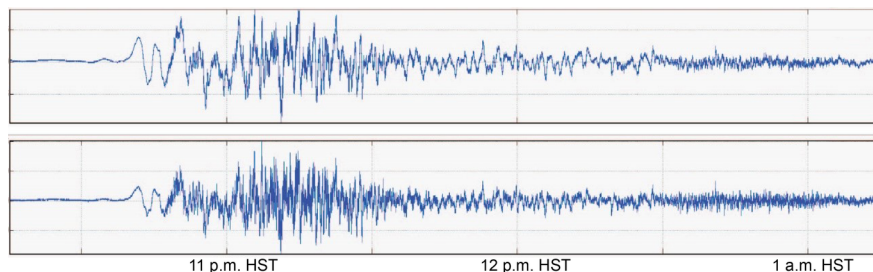


Figure 6: Pressure waves source from HTHH submarine volcano eruption on 15th January 2022 recorded by two USGS Hawaiian Volcano Observatory (HVO) infrasound sensors located south of Kīlauea volcano summit

Pressure waves from the event shows the highly compressional waves originated from the massive eruption that occurred on 15th January 2022. The nuclear bomb like explosion occurred at submarine volcano HTHH shows the flow of waves with a high velocity as shown in Fig. 6. There are various advantages to using HYSPLIT for volcanic ash monitoring. Firstly, by merging satellite retrievals with HYSPLIT models, it can enhance volcanic ash forecasts. Second, it can assist lessen the effects of volcanic ash on aircraft by giving precise ash deposition projections. Eventually, it may be utilised to account for aggregation in tephra-deposit model projections by adjusting particle-size distributions. Lastly, it can assist distinguish between phreatic and phreatomagmatic eruptions by offering insights into eruption mechanisms.

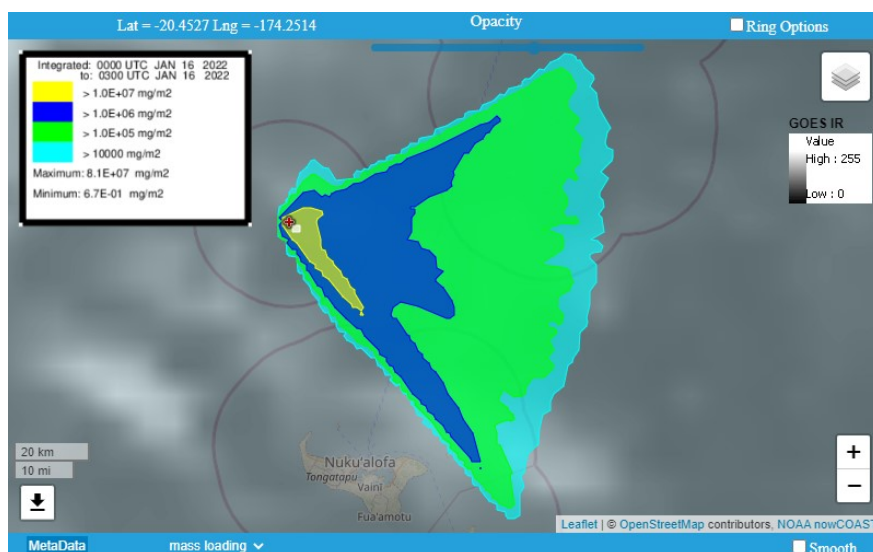


Figure 7: Shows volcanic ash particle deposition (mg/m^2) of 16th January 2022 after the massive eruption on 15 January 2022 at HTHH submarine volcano. This volcanic ash particle deposition (mg/m^2) plot obtained using READY of HYSPLIT by NOAA ARL

Overall, adopting HYSPLIT for volcanic ash monitoring is a useful technique for limiting the dangers posed by volcanic ash on flying aircraft. It gives precise volcanic ash deposition projections and aids in the differentiation of different types of eruptions.

3. Data, or a descriptive heading about data

HYSPLIT is a comprehensive system for simulating basic air parcel trajectories as well as sophisticated transport, dispersion, chemical transformation, and deposition scenarios. The HYSPLIT modelling system has already been used to track and forecast the release of radioactive material, wildfire smoke, windblown dust, pollutants from various stationary and mobile emission sources, allergies, volcanic ash, and simulation of atmospheric tracer release studies. The Air Resources Laboratory of NOAA created HYSPLIT. Volcanic ash cloud transport during the mid-week of the event has been simulated using HYSPLIT modelling system.

In this work, the HYSPLIT dispersion model is used to forecast volcanic ash movement and dispersion. To deliver information to VAACs, the National Weather Service (NWS) runs the HYSPLIT model with a unit mass release rate. The wind pattern above and around the volcano, on the other hand, is a key source of mistake in estimating where airborne volcanic ash will travel and settle. Scientists are employing satellite retrievals to incorporate data into the HYSPLIT model to enhance volcanic ash forecasts. Quantitative ash distribution projections may be given by objectively and ideally calculating the volcanic ash dispersal. MODIS satellite retrievals, for example, were used to assess the HYSPLIT model's performance in predicting the 2008 Kasatochi volcanic ash clouds.

Meteorological data files are accessible from a variety of sources, however the majority of them must be re-formatted before they can be used by HYSPLIT. Conversion applications in the HYSPLIT suite can be used to convert user-generated meteorological data to HYSPLIT format. In HYSPLIT, the Meteorology/Convert to ARL menu tab offers numerous choices for converting meteorological data. This data can be in Gridded Binary Format (only GRIB-1 is supported by the GUI), Network Common Data Form (NetCDF), or proprietary binary formats, such as NCAR's MM5.

HYSPLIT requires meteorological data at several heights and time periods across the simulation's lifetime on an equally spaced grid (latitude-longitude or conformal projection). The convert to ARL option in HYSPLIT

may convert gridded meteorological data on a latitude-longitude grid or one of three conformal projections to ARL format.

The HYSPLIT User's Handbook describes how to transform meteorological data for usage with HYSPLIT in detail. The manual offers context-sensitive assistance throughout the graphical user interface, commonly asked problems, and a list of utility tools such as file conversion and graphics creation. HYSPLIT is a full framework for calculating complicated dispersion and deposition trajectories. HYSPLIT requires meteorological data at several heights and time periods on an equally spaced grid (latitude-longitude or conformal projection) throughout the simulation. Meteorological data can be collected from a variety of sources that have already been prepared for use by HYSPLIT, or each user can convert their own data to the appropriate format.

NOAA provides source code and PC executable applications for converting meteorological data from diverse forms to a common format that HYSPLIT may use. NOAA also supplies UNIX converter programmes. The NOAA website provides access to HYSPLIT particle trajectories and footprint data. These data include footprints, which show locations where air parcels have come into touch with the Earth's surface within a specific time-period, and particle trajectories, which reflect an air parcel's passage across space through time.

In brief, HYSPLIT requires meteorological data on an equally spaced grid at several heights and time periods throughout the simulation. Meteorological data can be collected from a variety of sources that have already been prepared for use by HYSPLIT, or each user can convert their own data to the appropriate format.

4. Results, or a descriptive heading about the results

This model is designed to calculate the transport and dispersion of volcanic ash from the volcano peak to the column top. Within 0.1 degree of longitude, height, and latitude, the model estimates the position of computational particles. The accuracy of HYSPLIT output is based on the initialization accuracy: the beginning location, size distribution, and vertical profile of ash particles.

The HYSPLIT model performed interactively in this paper using the READY website and partially via script. The interactive map compares horizontal and vertical positioning, with colour denoting particle height. ARL based satellite data on volcanic ash clouds helps to enhance HYSPLIT volcanic ash forecasts. HYSPLIT simulation works for volcanic ash dispersion modelling as following conditions: eruption input, meteorological data input, ash particle distribution, ash cloud, reduced ash, and model output. In this work, the Windows-based HYSPLIT modelling system for volcanic- ash trajectories, ash particle deposition and ash particle position which includes single or multiple (space or time) simultaneous trajectories, optional grid of initial starting locations, computations forward or backward in time and default vertical motion using omega field. Ash particle position include motion options: isentropic, isosigma, isobaric and isopycnic in which trajectory ensemble using meteorological variations and the output of meteorological variables along a trajectory and trajectory clustering option for volcanic ash particle deposition.

Using HYSPLIT modelling system we get below results from the simulation with Fig.7. which include figures i-v showing the volcanic ash particle deposition from the multiple eruptions that happened on 14th January 2022 to 18th January 2022 at submarine volcano HTHH. Figures vi-x shows the volcanic ash particle trajectories and figures xi-xv illustrates the ash particle positions from the same series of multiple eruptions occurred at HTHH submarine volcano.

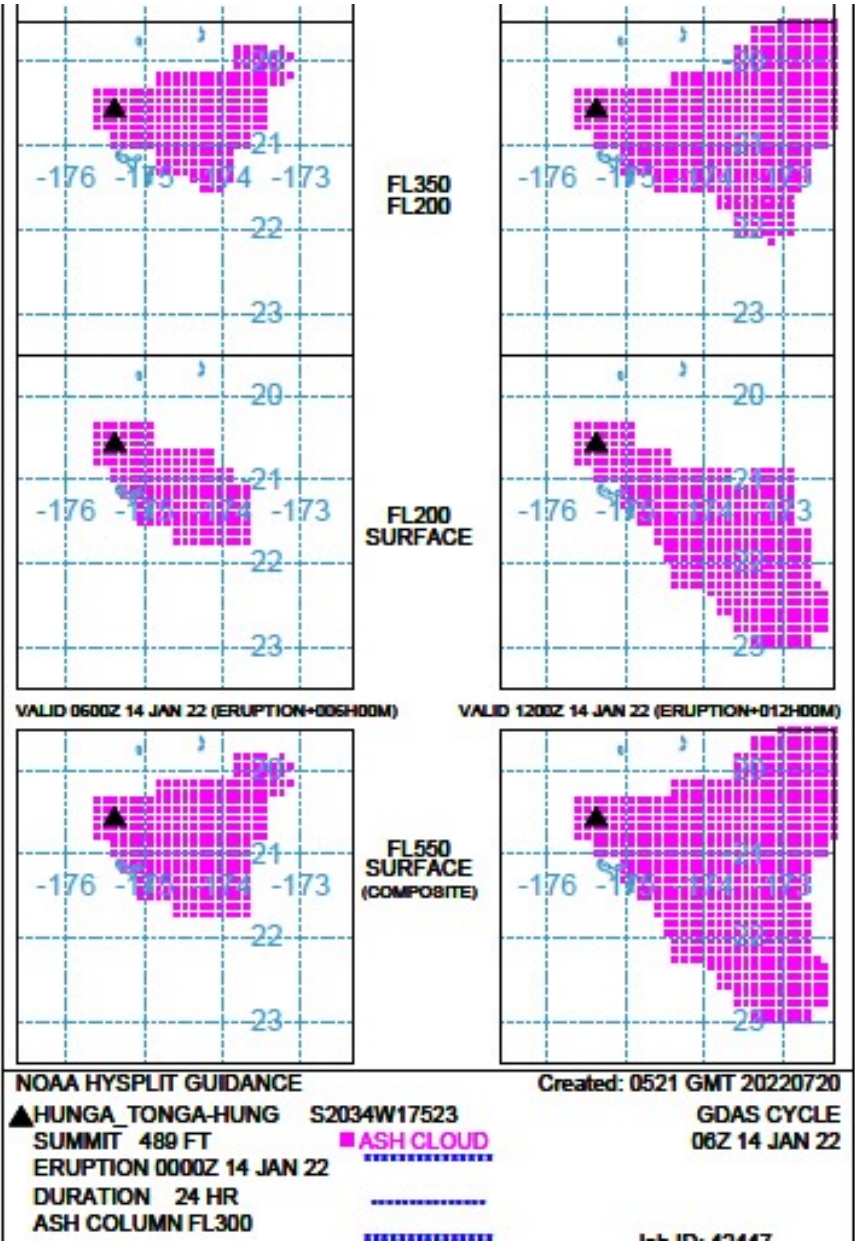


Figure 8: (i)

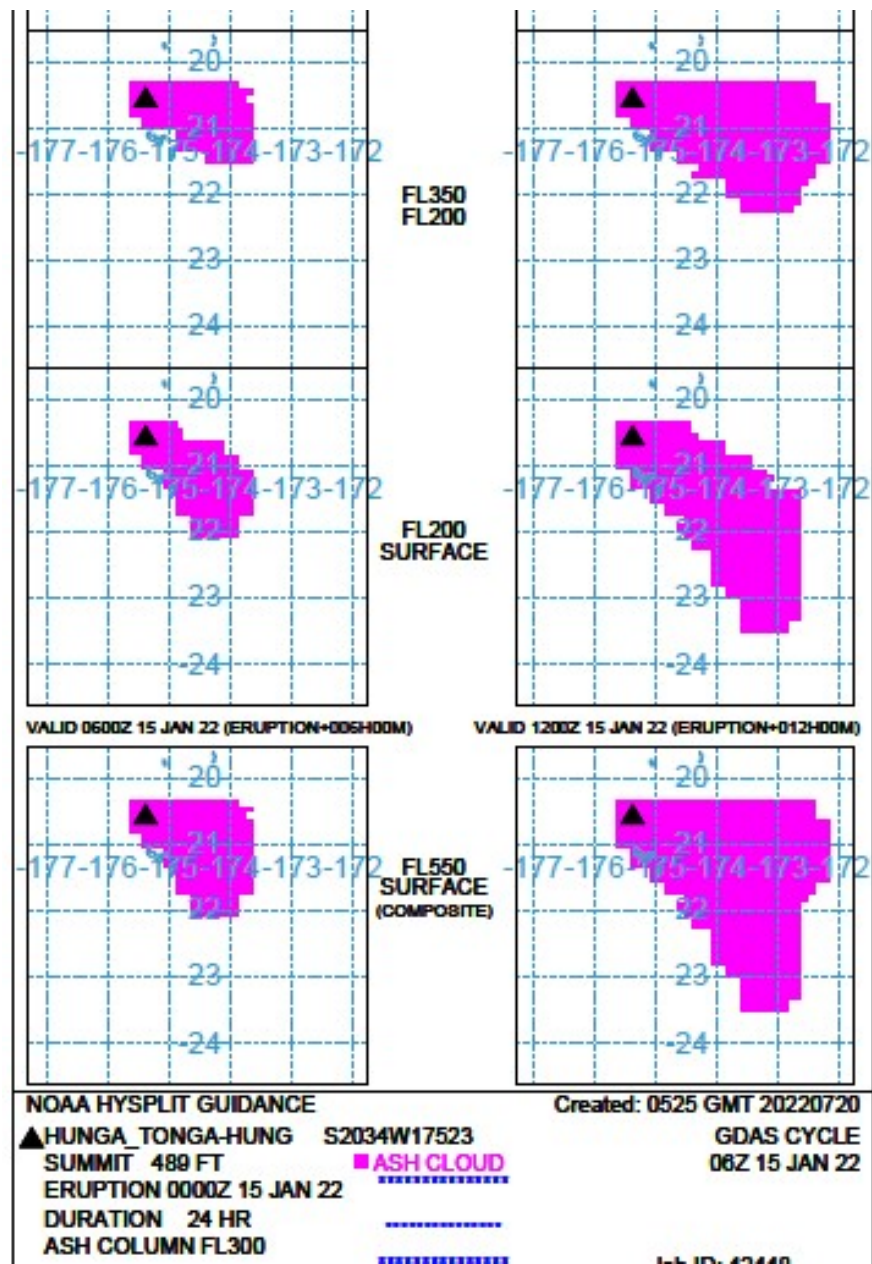


Figure 9: (ii)

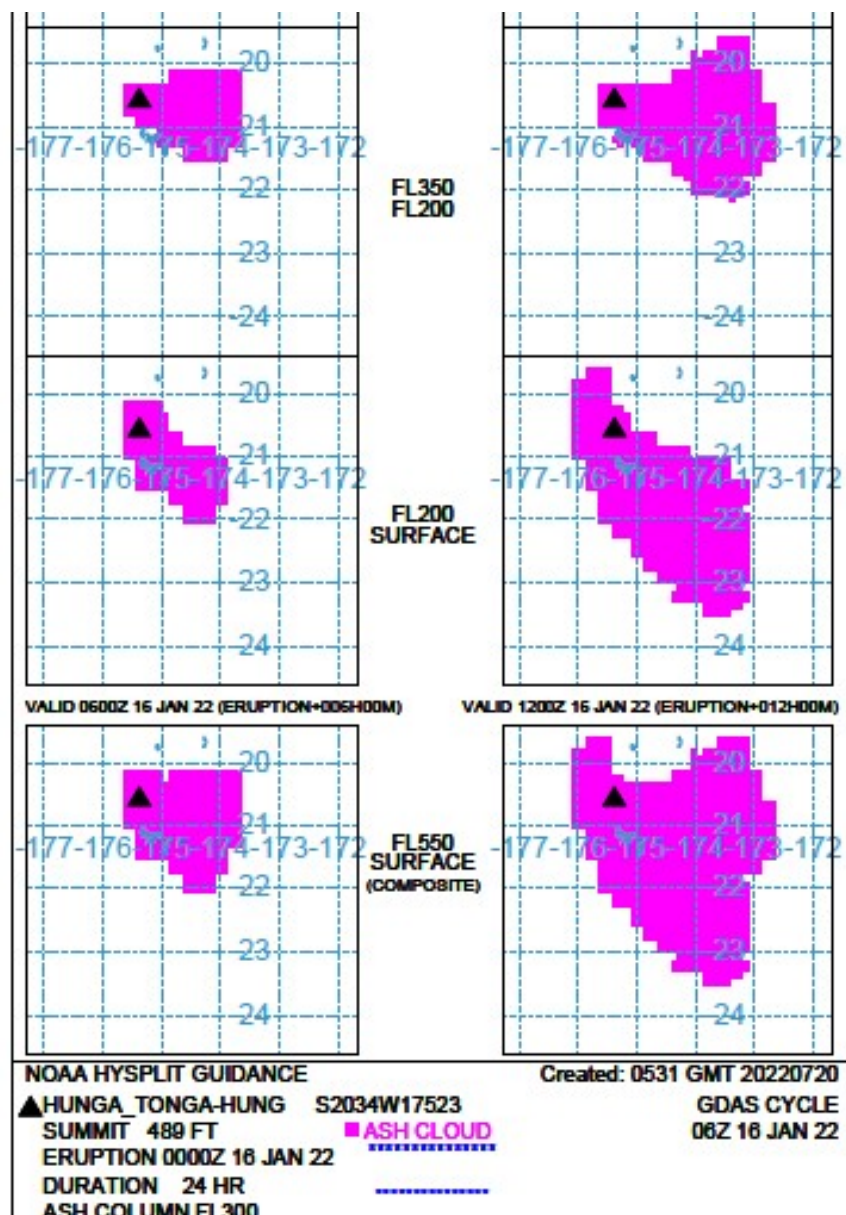


Figure 10: (iii)

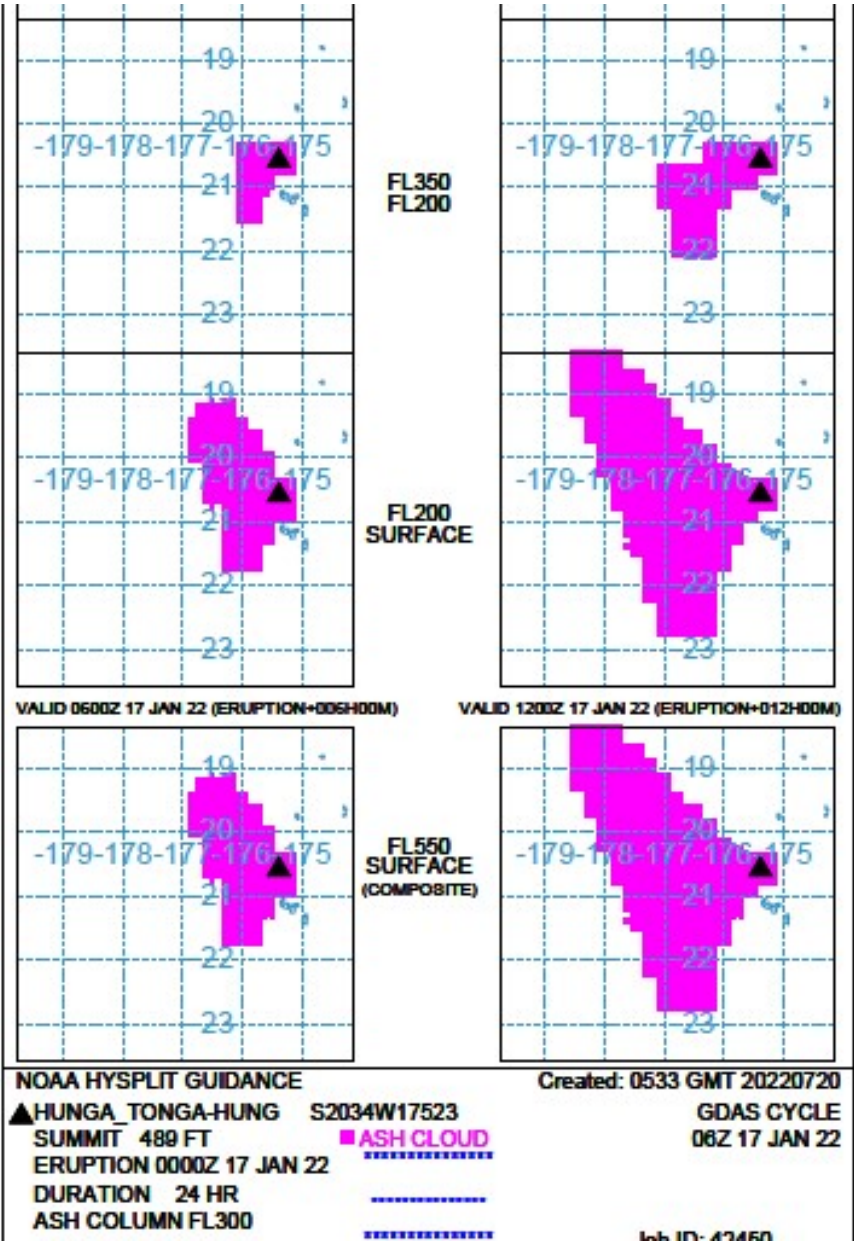


Figure 11: (iv)

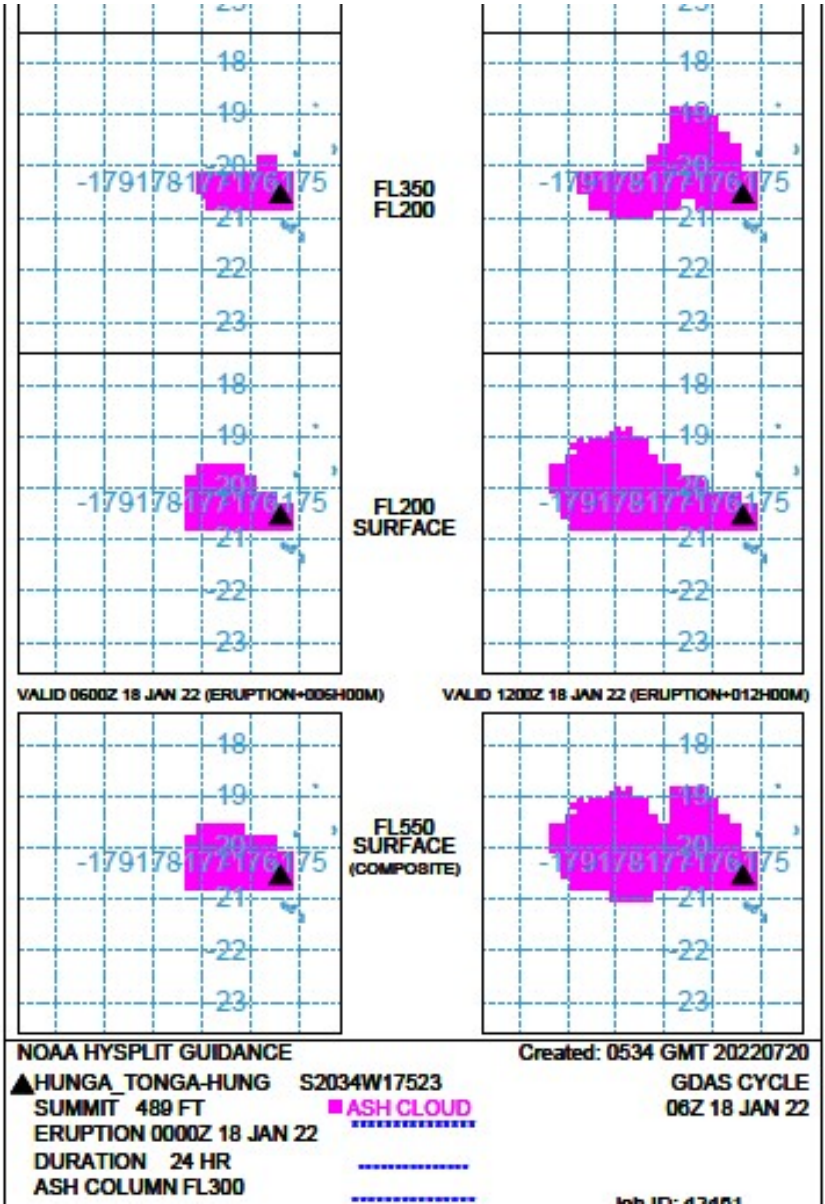
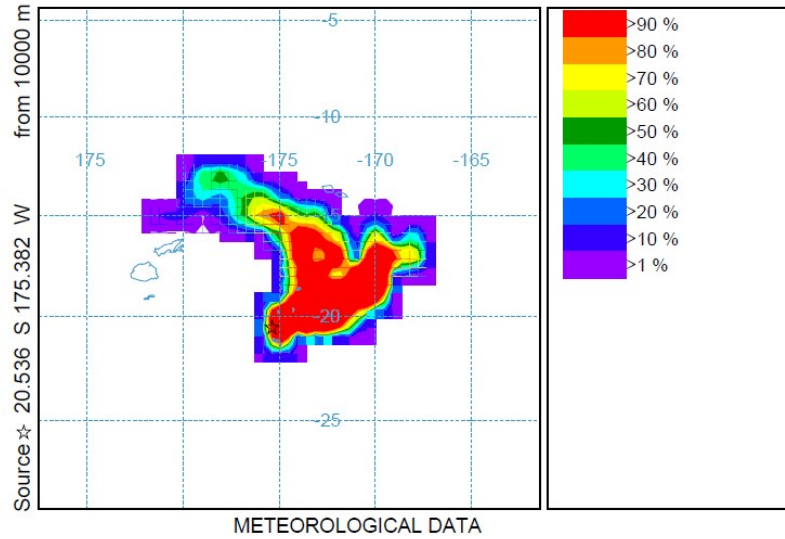


Figure 12: (v)

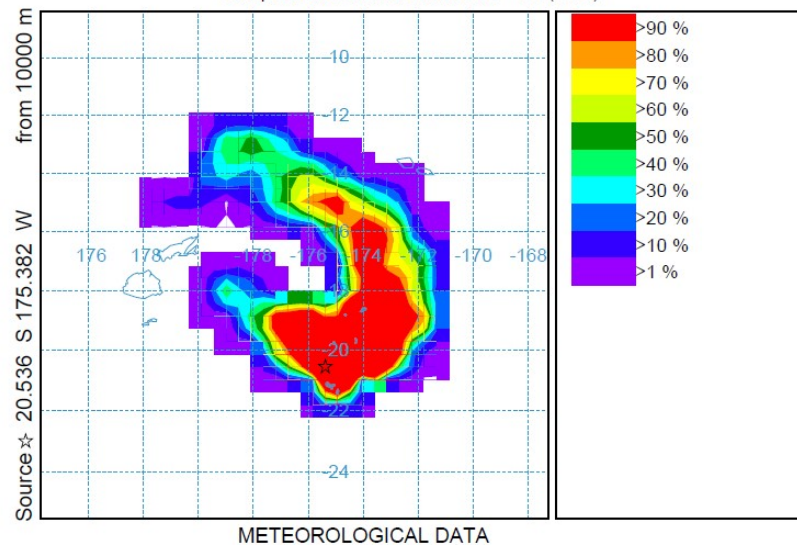
NOAA HYSPLIT MODEL - TRAJECTORY FREQUENCIES

endpts per grid sq./# trajectories (%) 0 m and 99999 m
Integrated from 0000 14 Jan to 1800 17 Jan 22 (UTC)
Freq Release started at 0000 00 00 (UTC)



NOAA HYSPLIT MODEL - TRAJECTORY FREQUENCIES

endpts per grid sq./# trajectories (%) 0 m and 99999 m
Integrated from 0000 15 Jan to 1800 18 Jan 22 (UTC)
Freq Release started at 0000 00 00 (UTC)



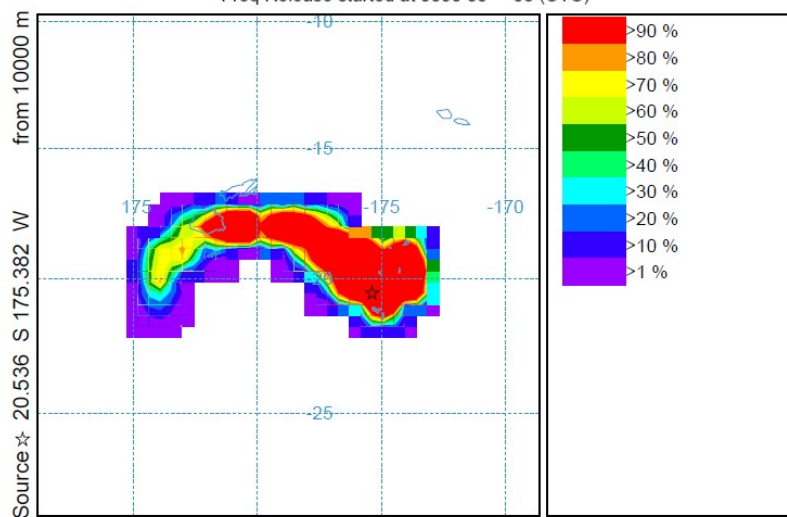
(vi) and (vii)

NOAA HYSPLIT MODEL - TRAJECTORY FREQUENCIES

endpts per grid sq./# trajectories (%) 0 m and 99999 m

Integrated from 0000 16 Jan to 1800 19 Jan 22 (UTC)

Freq Release started at 0000 00 00 (UTC)

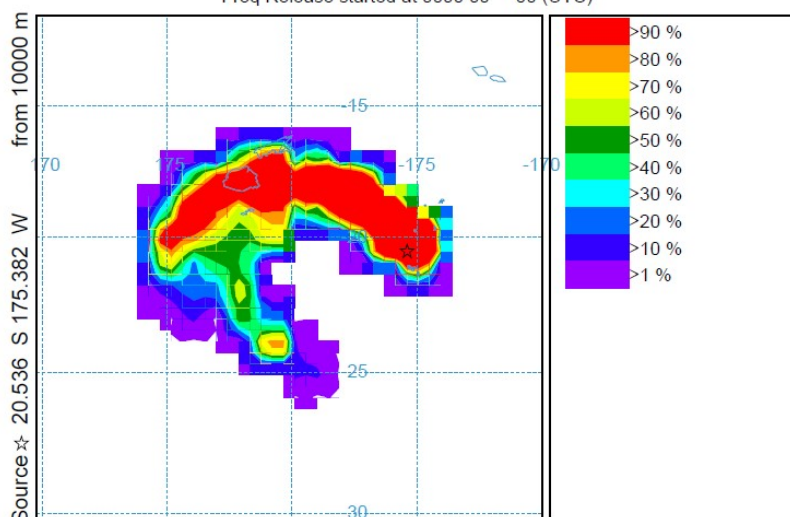


NOAA HYSPLIT MODEL - TRAJECTORY FREQUENCIES

endpts per grid sq./# trajectories (%) 0 m and 99999 m

Integrated from 0000 17 Jan to 1800 20 Jan 22 (UTC)

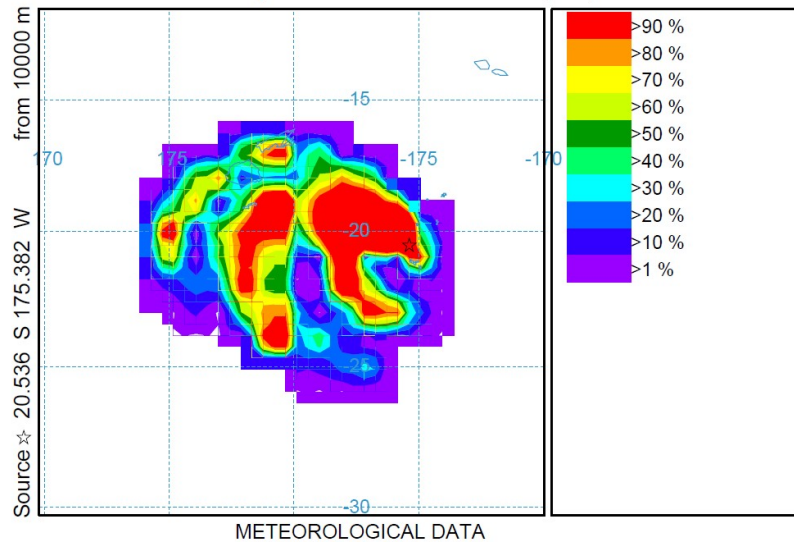
Freq Release started at 0000 00 00 (UTC)



(viii) and (ix)

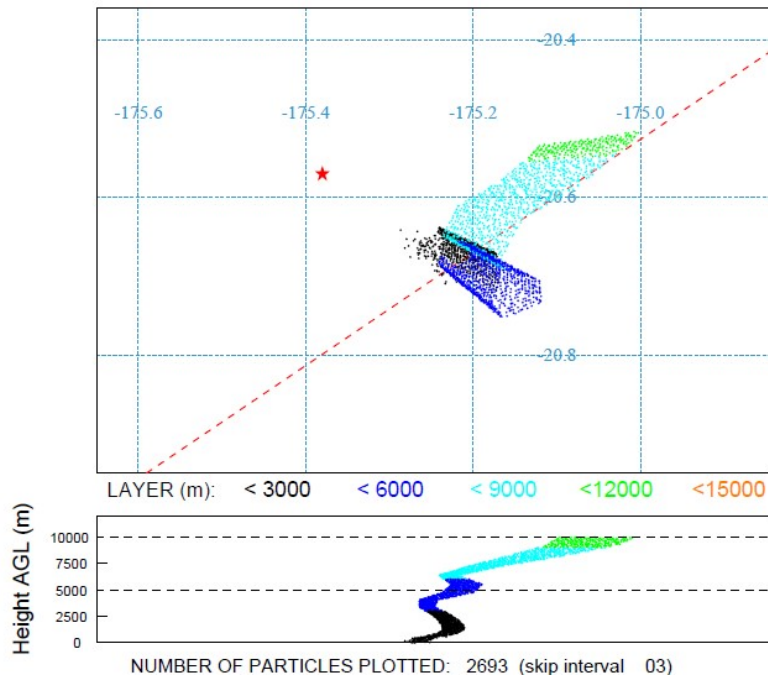
NOAA HYSPLIT MODEL - TRAJECTORY FREQUENCIES

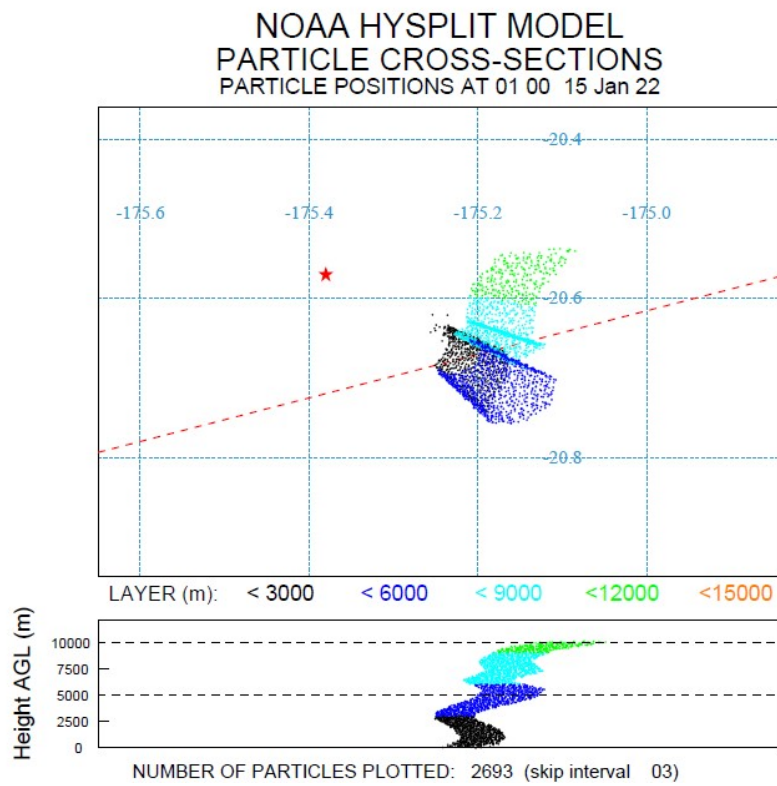
endpts per grid sq./# trajectories (%) 0 m and 99999 m
Integrated from 0000 18 Jan to 1800 21 Jan 22 (UTC)
Freq Release started at 0000 00 00 (UTC)



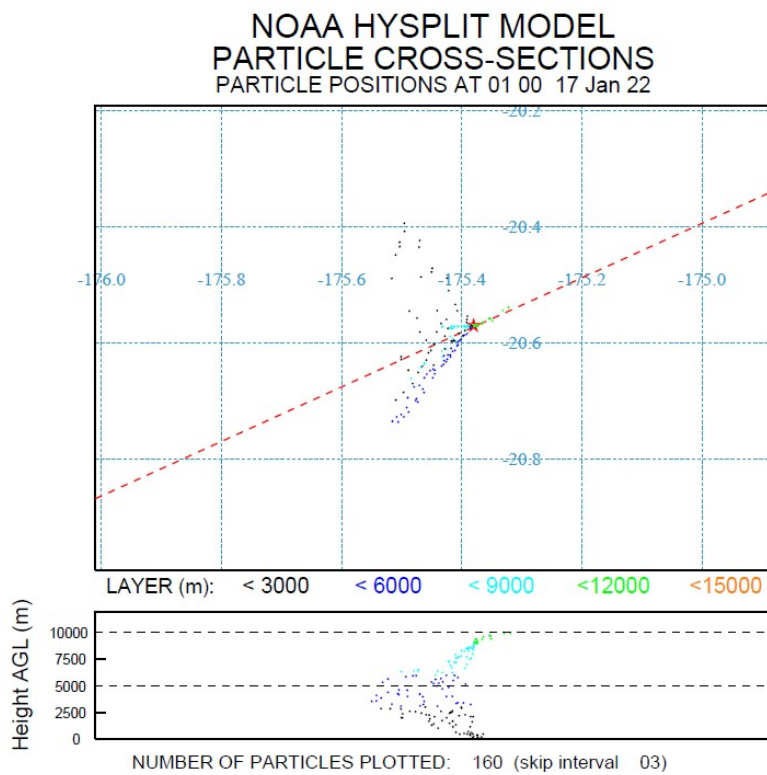
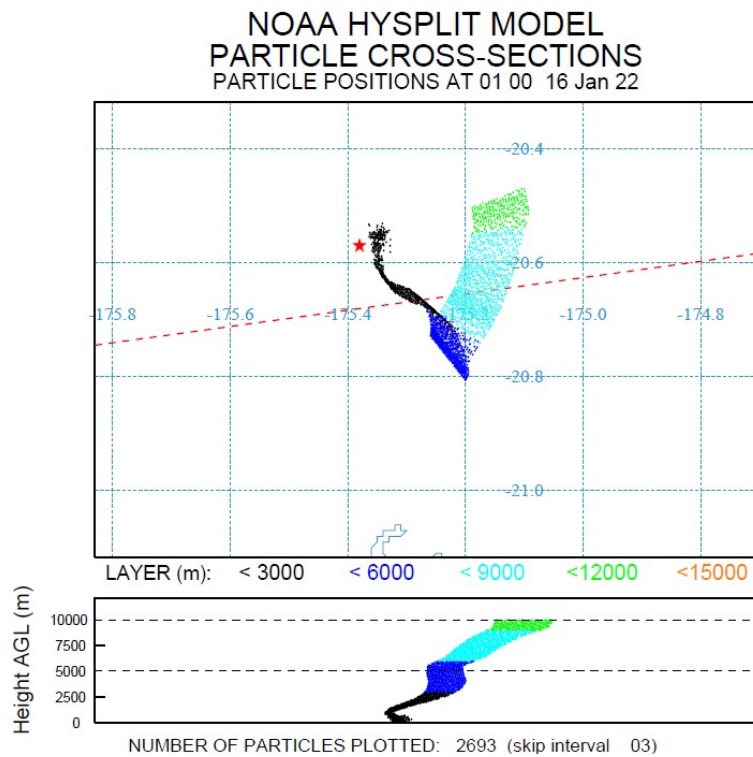
(x)

NOAA HYSPLIT MODEL PARTICLE CROSS-SECTIONS PARTICLE POSITIONS AT 01 00 14 Jan 22





(xi) and (xii)



(xiii) and (xiv)

Below (xv)

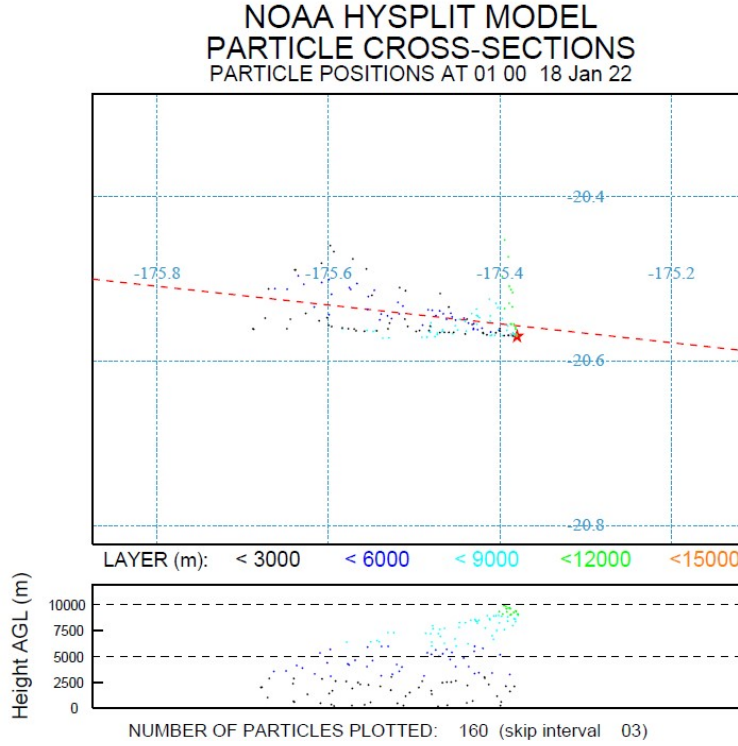


Figure 13: Figures (i-v or 8-12) shows the volcanic ash particle deposition occurred on 14th January 2022 to 18th January 2022 at HTHH submarine volcano multiple eruptions. Figures (vi-x) depicts the volcanic ash particle trajectories from the same event and figures (xi-xv) for the ash particle positions that occurred between 14-18 January 2022 at HTHH submarine volcano.

5. Conclusions

In this paper, the simulation results have been analysed. The simulations estimated using HYSPLIT modelling system has been carried out for submarine HTHH volcano activity from 14th January to 18th January 2022 (mid-week of January 2022 focusing the multiple eruption events. The investigations specifically based on:

- volcanic ash particle deposition,
- volcanic ash particle trajectories, and
- volcanic ash particle positions.

The results from the simulations can be divided into two parts basically with the pre-caldera volcanic activity, i.e., before massive eruption on 15th January 2022. The simulations of 14th January 2022 for volcanic ash particle - deposition, trajectories and particle position can be coined as ‘pre-caldera’ volcanic activity. Generally during ‘pre-caldera’ volcanic activity several more eruptions, including lava flows, ash plumes, and explosive eruptions, may occur during the pre-caldera period of the volcano. The scale of the

volcano may grow over time as more material is added to the cone, and the eruption types may vary as the magma chamber underneath the volcano changes.

Investigations for pre-caldera volcanic activity gain a better understanding of the processes that lead up to a big eruption and to try to forecast when a volcanic caldera will form. Seismometers, GPS equipment, gas sensors, and satellite photos usually use to precisely monitor the volcano's behaviour and follow any changes in activity. The collapse of the top may create a new conduit for magma to reach the surface, resulting in a fresh period of volcanic activity after the construction of a caldera. Furthermore, the collapse may expose new weak points in the volcano's structure, rendering it more vulnerable to future eruptions. Yet, depending on the exact volcano and the surrounding geology, the specific conditions that contribute to post-caldera volcanic activity might vary greatly.

The HYSPLIT modelling system for HTHH submarine volcanic activity in the mid-week of January 2022 multiple eruptions has been focused to get clearance reports from the simulated results in order to make volcanic ash forecasting results more visualized. Based on the eruption event simulations HYSPLIT modelling system proves that how monitoring system parameters are in operations and how the forecasting analyser works with the HTHH submarine volcanic activity data set for multiple eruptions.

Fig. 8 (figures xi-xv), comprises the volcanic ash particle positions of submarine HTHH volcanic activity before and after massive eruption occurred on 15th January 2022. The volcanic ash particles go <12000 m layer (AGL) on 14th January 2022 simulation result as in Fig. 8. of figure xi, whereas figure xii-xv the post-caldera state starts after the massive eruption on 15th January 2022 the ash particles go >12000 m layer of AGL. The volcanic ash particle trajectories, fig. 8 (figures vi-x) shows the ash particle deposition level in the stratosphere goes >90% even before and after the massive eruption event of 15th January 2022. HYSPLIT outputs have more detailed impression of accuracy that's why the large uncertainties in the eruption parameters i.e., the volcanic ash particle deposition has shown impact as seen in Fig. 8 (figures i-v) where the ash cloud composite increased by 75% after the massive eruption on 15th January 2022 where the difference can be clearly visible in Fig. 8 (figures i, iii and iv). More than 300,000 volcanic trace particles per day were released during the multiple eruption times of mid-week of January 2022 and can be seen from the simulation results.

6. Future Accomplishments

In our study, we focused on utilizing the HYSPLIT modelling system with GDAS meteorological data, volcanic ash cloud composite, ash cloud trajectory frequency, and ash particle positions, which are discussed in Section 4 of the paper. Additionally, we generated event time seismograms using PyWEED, as shown in Figure 3.

Regarding seismic activity in the Czech Republic, there is potential for implementing a machine learning-based sensing system using optical fibres as seismic sensors. In the western part of the country, particularly in the Nový Kostel region, there is a history of frequent earthquakes with magnitudes below 4 occurring throughout the year. This presents an opportunity for deploying new fibre sensing methods in our country, as we have access to optical fibre lines that are commonly shared for research activities. Dedicated parts of the spectrum are being tested for various research transmissions, including sensing, QKD (Quantum Key Distribution), and Precise Time and Frequency transfers, leaving room for cost-efficient solutions for future research endeavours.

Collaboration with well-established and recognized volcano regions, which possess comprehensive sensing data, could provide valuable insights and more precise methods for volcanology. Optical fibre sensing methods offer the potential for acquiring essential data on gas content and composition in seismic activity regions worldwide.

The CESNET2 network in the Czech Republic already applies advanced applications for sensing in the Temelín nuclear power plant, specifically for containment stability measurements. This involves ultra-stable frequency transfers between the National Metrology Institution and the containment sensors. While the

project primarily focuses on the stability of the containment itself, it also considers seismic events, including earthquakes.

To compare the situation during the eruption events of the HTHH submarine volcano, we examined seismic activity on the other side of the Earth, specifically in central Europe, where our locality is situated. Figure 9 demonstrates a seismograph recording an earthquake activity with a magnitude of 2.8 at 02:54:47 UTC on January 15th, 2022, near the Aschach area, northwest of Linz. This earthquake activity was also monitored for the safety of the nearby Temelín nuclear power plant. Although these seismic activities generally have "low" magnitudes, they tend to be long-lasting and occur throughout the year. CESNET, as the Czech NREN (National Research and Education Network) provider, actively engages with advanced technologies to achieve more precise measurements and is open to further collaboration within the field.

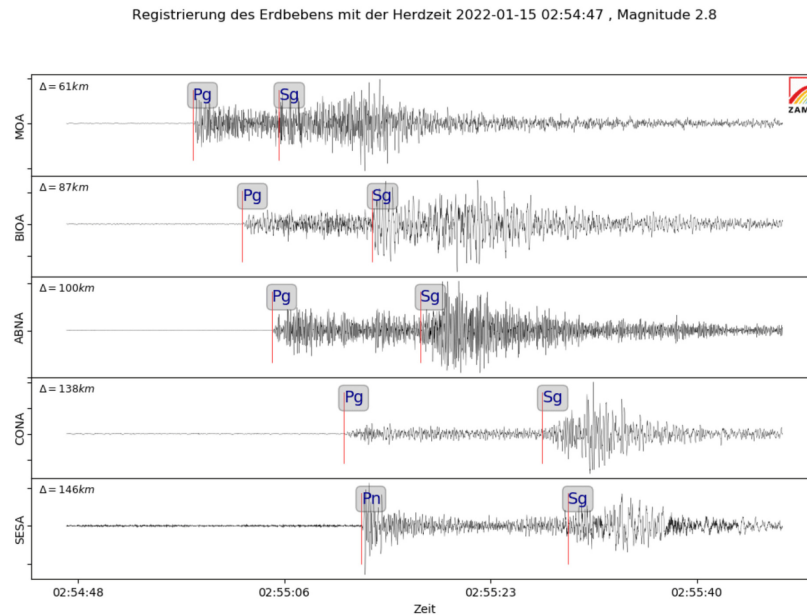


Fig. 9. Seismograph of 2.8 (ML) near Aschach, north-west of Linz., Austria near the border of Czech Republic (15th January 2022, 02:54:47 UTC)

Acknowledgments

This work is partially supported by Ministry of Education, Youth and Sport of the Czech Republic by the project "E infrastructure CESNET-modernization", reg. no. CZ.02.1.01/0.0/0.0/16.013/0001797 and in part by the TiFOON 18SIB06 Project through the EMPIR Programme co-financed by the participating states.

References

- Biggs, J., Ayele, A., Fischer, T.P. et al. (2021), Volcanic activity and hazard in the East African Rift Zone. *Nat Commun* 12, 6881. <https://doi.org/10.1038/s41467-021-27166-y>
- A. M. Crawford, B. J. B. Stunder, F. Ngan, M. J. Pavolonis, 2016. Initializing HYSPLIT with satellite observations of volcanic ash: A case study of the 2008 Kasatochi eruption, *J. Geophys. Res. Atmos.*, 121, doi:10.1002/2016JD024779.

T. Chai, A. Crawford, B. J. B. Stunder, M. J. Pavolonis, R. Draxler, A. Stein, 2017. Improving volcanic ash predictions with the HYSPLIT dispersion model by assimilating MODIS satellite retrievals, *Atmos. Chem. Phys.*, 17, <https://doi.org/10.5194/acp-17-2865-2017>

Crawford, A.: The Use of Gaussian Mixture Models with Atmospheric Lagrangian Particle Dispersion Models for Density Estimation and Feature Identification. *Atmosphere* 2020, 11, 1369. <https://doi.org/10.3390/atmos11121369>

Masterin, L.G., M. Guffanti, R. Servranckx, P. Webley, S. Barsotti, K. Dean, A. Durant, J.W. Ewert, A. Neri, W.I. Rose, D. Schneider, L. Siebert, B. Stunder, G. Swanson, A. Tupper, A. Volentik, C.F. Waythomas, 2009: A multidisciplinary effort to assign realistic source parameters to models of volcanic ash-cloud transport and dispersion during eruptions *Journal of Volcanology and Geothermal Research*, 186:10-21.

Webley, P.W., B.J.B. Stunder, and K.G. Dean. 2009: Preliminary sensitivity study of eruption source parameters for operational volcanic ash cloud transport and dispersion models — A case study of the August 1992 eruption of the Crater Peak vent, Mount Spurr, Alaska. *Journal of Volcanology and Geothermal Research*, 186:108-119.

Stunder, B.J.B., J.L. Heffter, R.R. Draxler (2007), Airborne Volcanic Ash Forecast Area Reliability, *Weather and Forecasting*, 22:1132-1139, DOI: 10.1175/WAF1042.1

Tupper, A., J. Davey, P. Stewart, B. Stunder, R. Servranckx, and F. Prata, 2006: Aircraft encounters with volcanic clouds over Micronesia, Oceania, 2002/03. *Australian Meteorological Magazine*, 55, 289-299.

Heffter, J.L., 1996: Volcanic ash model verification using a Klyuchevskoi eruption. *Geophys. Res. Letters*, 23-12, 1489-1492. Heffter, J.L. and B.J.B. Stunder, 1993: Volcanic Ash Forecast Transport And Dispersion (VAFTAD) Model. *Weather Forecasting*, 8, 534-541.

Heffter, J.L., B.J.B. Stunder, and G.D. Rolph, 1990: Long-range forecast trajectories of volcanic ash from Redoubt volcano eruptions. *Bull. Amer. Meteor. Soc.* 71(12):1731-1738.

Stunder, B.J.B., J.L. Heffter, R.R. Draxler (2007), Airborne Volcanic Ash Forecast Area Reliability, *Weather and Forecasting*, 22:1132-1139, DOI: 10.1175/WAF1042.1

Tupper, A., J. Davey, P. Stewart, B. Stunder, R. Servranckx, and F. Prata, 2006: Aircraft encounters with volcanic clouds over Micronesia, Oceania, 2002/03. *Australian Meteorological Magazine*, 55, 289-299.

Heffter, J.L., 1996: Volcanic ash model verification using a Klyuchevskoi eruption. *Geophys. Res. Letters*, 23-12, 1489-1492.

Heffter, J.L. and B.J.B. Stunder, 1993: Volcanic Ash Forecast Transport And Dispersion (VAFTAD) Model. *Weather Forecasting*, 8, 534-541.

Heffter, J.L., B.J.B. Stunder, and G.D. Rolph, 1990: Long-range forecast trajectories of volcanic

ash from Redoubt volcano eruptions. *Bull. Amer. Meteor. Soc.* 71(12):1731-1738.

Rolph, G., Stein, A., & Stunder, B. (2017). Real-time environmental applications and display system: READY. *Environmental Modelling & Software*, 95, 210-228.
<https://doi.org/10.1016/j.envsoft.2017.06.025>

AWS, 1979. The Use of the Skew of T, log P Diagram in Analysis and Forecasting. AWS/TR-79/006, Air Weather Service, Scott AFB, IL, 150 pp. [Available from: Air Weather Service (MAC), Scott AFB, IL 62225].

Draxler, R.R., 1979. Estimating vertical diffusion from routine meteorological tower measurements. *Atmos. Environ.* 13, 1559e1564.
[http://dx.doi.org/10.1016/0004-6981\(79\)90065-9](http://dx.doi.org/10.1016/0004-6981(79)90065-9)

Draxler, R.R., 1982. Measuring and modelling the transport and dispersion of kRYPTON-85 1500km from a point source. *Atmos. Environ.* 16, 2763e2776.
[http://dx.doi.org/10.1016/0004-6981\(82\)90027-0](http://dx.doi.org/10.1016/0004-6981(82)90027-0)

Draxler, R.R., 1996. Trajectory optimization for balloon flight planning. *Wea. Forecast.* 11, 111e114
[http://dx.doi.org/10.1175/1520-0434\(1996\)011<0111:TOFBFP>2.0.CO;2](http://dx.doi.org/10.1175/1520-0434(1996)011<0111:TOFBFP>2.0.CO;2)

Draxler, R.R., 1999. HYSPLIT4 User's Guide. NOAA Tech. Memo. ERL ARL-230, 35 pp. [2016 version available online at: http://www.arl.noaa.gov/documents/reports/hysplit_user_guide.pdf. last access: January 2016].

Draxler, R.R., Hess, G.D., 1998. An overview of the HYSPLIT 4 modelling system for trajectories, dispersion, and deposition. *Aust. Meteor. Mag.* 47, 295e308.

Kalnay, E., Kanamitsu, M., Kistler, R., Collins, W., Deaven, D., Gandin, L., Iredell, M., Saha, S., White, G., Woollen, J., Zhu, Y., Chelliah, M., Ebisuzaki, W., Higgins, W., Janowiak, J., Mo, K.C., Ropelewski, C., Wang, J., Leetmaa, A., Reynolds, R., Jenne, R., Joseph, D., 1996. The NCEP/NCAR 40-year Reanalysis project. *Bull. Am. Met. Soc.* 77, 437e471
[http://dx.doi.org/10.1175/1520-0477\(1996\)077<0437:TNYP>2.0.CO;2](http://dx.doi.org/10.1175/1520-0477(1996)077<0437:TNYP>2.0.CO;2)

Ngan, F., Stein, A., 2017. A long-term WRF meteorological archive for dispersion simulations: application to controlled tracer experiments. *J. Appl. Meteor. Climatol.*
<http://dx.doi.org/10.1175/JAMC-D-16-0345.1> in press.

Ngan, F., Stein, A.F., Draxler, R.R., 2015. Inline coupling of WRF-HYSPLIT: model development and evaluation using tracer experiments. *J. Appl. Meteor. Climatol.* 54, 1162e1176. <http://dx.doi.org/10.1175/JAMC-D-14-0247.1>

Solazzo, E., Galmarini, S., 2014. The Fukushima-137Cs deposition case study: properties

of the multi-model ensemble. *J. Environ. Radioact.* 139, 226e233.
<http://dx.doi.org/10.1016/j.jenvrad.2014.02.017>

Stein, A.F., Draxler, R.R., Rolph, G.D., Stunder, B.J.B., Cohen, M.D., Ngan, F., 2015. NOAA's HYSPLIT atmospheric transport and dispersion modelling system. *Bull. Am. Meteorol. Soc.* 96, 2059e2077. <http://dx.doi.org/10.1175/BAMS-D-14-00110.1>

WMO, 2014. Documentation on RSMC Support for Environmental Emergency Response. Technical Document WMO-TD/No.778. World Meteorological Organization, Geneva, Switzerland. Available online at:
<http://www.wmo.int/pages/prog/www/DPFSERA/td778.html>

Millán, L., Santee, M. L., Lambert, A., Livesey, N. J., Werner, F., Schwartz, M. J., et al. (2022). The Hunga Tonga-Hunga Ha'apai Hydration of the Stratosphere. *Geophysical Research Letters*, 49, e2022GL099381. <https://doi.org/10.1029/2022GL099381>

Harding, B. J., Wu, Y.-J. J., Alken, P., Yamazaki, Y., Triplett, C. C., Immel, T. J., et al. (2022). Impacts of the January 2022 Tonga volcanic eruption on the ionospheric dynamo: ICON-MIGHTI and Swarm observations of extreme neutral winds and currents. *Geophysical Research Letters*, 49, e2022GL098577. <https://doi.org/10.1029/2022GL098577>

Schnepf, N. R., Minami, T., Toh, H., & Nair, M. C. (2022). Magnetic signatures of the 15 January 2022 Hunga Tonga–Hunga Ha'apai volcanic eruption. *Geophysical Research Letters*, 49, e2022GL098454. <https://doi.org/10.1029/2022GL098454>

Astafyeva, E., Maletckii, B., Mikesell, T. D., Munaibari, E., Ravanelli, M., Coisson, P., et al. (2022). The 15 January 2022 Hunga Tonga eruption history as inferred from ionospheric observations. *Geophysical Research Letters*, 49, e2022GL098827. <https://doi.org/10.1029/2022GL098827>

Legas, B., Duchamp, C., Sellitto, P., Podglajen, A., Carboni, E., Siddans, R., Groß, J., Khaykin, S., & Ploeger, F. (2022). The evolution and dynamics of the Hunga Tonga plume in the stratosphere. <https://doi.org/10.5194/egusphere-2022-517>

D'Arcangelo, S.; Bonforte, A.; De Santis, A.; Maugeri, S.R.; Perrone, L.; Soldani, M.; Arena, G.; Brogi, F.; Calcara, M.; Campuzano, S.A.; et al. A Multi-Parametric and Multi-Layer Study to Investigate the Largest 2022 Hunga Tonga–Hunga Ha'apai Eruptions. *Remote Sens.* 2022, 14, 3649. <https://doi.org/10.3390/rs14153649>

Mishra, M.K.; Hoffmann, L.; Thapliyal, P.K. Investigations on the Global Spread of the Hunga Tonga-Hunga Ha'apai Volcanic Eruption Using Space-Based Observations and Lagrangian Transport Simulations. *Atmosphere* 2022, 13, 2055. <https://doi.org/10.3390/atmos13122055>

Garvin, J. B., Slayback, D. A., Ferrini, V., Frawley, J., Giguere, C., Asrar, G. R., & Andersen, K.

- (2018). Monitoring and modelling the rapid evolution of Earth’s newest volcanic island: Hunga Tonga Hunga Ha’apai (Tonga) using high spatial resolution satellite observations. *Geophysical Research Letters*, 45, 3445–3452. <https://doi.org/10.1002/2017GL076621>
- Wohletz, K., & Heiken, G. (1992). *Volcanology and geothermal energy*.
- Hurst, T., & Davis, C. (2017). Forecasting volcanic ash deposition using HYSPLIT. *Journal of Applied Volcanology*, 6(1). <https://doi.org/10.1186/s13617-017-0056-7>
- Xu, J.; Li, D.; Bai, Z.; Tao, M.; Bian, J. Large Amounts of Water Vapor Were Injected into the Stratosphere by the Hunga Tonga–Hunga Ha’apai Volcano Eruption. *Atmosphere* 2022, 13, 912. <https://doi.org/10.3390/atmos13060912>
- Brenna, M., Cronin, S., Smith, I., Pontesilli, A., Tost, M., Barker, S., & Tongaonevai, S. (2022). Post-caldera volcanism reveals shallow priming of an intra-ocean arc andesitic caldera: Hunga volcano, Tonga, SW Pacific. <https://doi.org/10.31223/x5qp8v>
- Plank, S., Marchese, F., Genzano, N., Nolde, M., & Martinis, S. (2020). The short life of the volcanic island new Late’iki (Tonga) analyzed by multi-sensor remote sensing data. *Scientific Reports*, 10(1). <https://doi.org/10.1038/s41598-020-79261-7>
- Chouet, B., P. Dawson, T. Ohminato, M. Martini, G. Saccorotti, F. Giudicepietro, G. De Luca, G. Milana, and R. Scarpa, Source mechanisms of explosions at Stromboli Volcano, Italy, determined from moment-tensor inversions of very-long-period data, *J. Geophys. Res.*, 108(B1), 2019, doi:10.1029/2002JB001919, 2003.
- Wassermann J (2012) Volcano seismology. In: Peter B (ed) IASPEI new manual of seismological observatory practice 2 (NMSOP-2), second. Potsdam : Deutsches GeoForschungsZentrum GFZ, Potsdam, pp 1–77. doi:10.2312/GFZ.NMSOP-2_ch13
- Saccorotti, G., & Lokmer, I. (2021). A review of seismic methods for monitoring and understanding active volcanoes. *Forecasting and Planning for Volcanic Hazards, Risks, and Disasters*, 25-73. <https://doi.org/10.1016/b978-0-12-818082-2.00002-0>
- Chouet, B. A., & Matoza, R. S. (2013). A multi-decadal view of seismic methods for detecting precursors of magma movement and eruption. *Journal of Volcanology and Geothermal Research*, 252, 108-175. <https://doi.org/10.1016/j.jvolgeores.2012.11.013>
- Lomax, A., & Michelini, A. (2009). Tsunami early warning using earthquake rupture duration. *Geophysical Research Letters*, 36(9). <https://doi.org/10.1029/2009gl037223>
- Andy Jurkevics; Polarization analysis of three-component array data. *Bulletin of the Seismological Society of America* 1988;; 78 (5): 1725–1743. doi:<https://doi.org/10.1785/BSSA0780051725>
- Jousset, P., Budi-Santoso, A., Jolly, A. D., Boichu, M., Surono, Dwiyo, S., Sumarti, S., Hidayati, S., & Thierry, P. (2013). Signs of magma ascent in LP and VLP seismic events and link to degassing: An example from the 2010 explosive eruption at Merapi volcano, Indonesia. *Journal of Volcanology and Geothermal Research*, 261, 171-192. <https://doi.org/10.1016/j.jvolgeores.2013.03.014>
- Soubestre, J., Shapiro, N. M., Seydoux, L., de Rosny, J., Droznin, D. V., Droznina, S. Y., Gordeev, E. I. (2018). Network-based detection and classification of seismovolcanic tremors: Example from

the Klyuchevskoy volcanic group in Kamchatka. *Journal of Geophysical Research: Solid Earth*, 123.<https://doi.org/10.1002/2017JB014726>

Rost, S., & Thomas, C. (2002). Array seismology: Methods and applications. *Reviews of Geophysics*, 40(3), 2-1-2-27.<https://doi.org/10.1029/2000rg000100>

Wassermann, J., Braun, T., Ripepe, M., Bernauer, F., Guattari, F., & Igel, H. (2022). The use of 6DOF measurement in volcano seismology – A first application to Stromboli volcano. *Journal of Volcanology and Geothermal Research*, 424, 107499.<https://doi.org/10.1016/j.jvolgeores.2022.107499>

Thomson, D. J. (1987). Criteria for the selection of stochastic models of particle trajectories in turbulent flows. *Journal of Fluid Mechanics*, 180(-1), 529.<https://doi.org/10.1017/s0022112087001940>

Shao, Y., Hacker, J. M., & Schwerdtfeger, P. (1991). The structure of turbulence in a coastal atmospheric boundary layer. *Quarterly Journal of the Royal Meteorological Society*, 117(502), 1299-1324.<https://doi.org/10.1002/qj.49711750209>

Reynolds AM. Incorporating terminal velocities into Lagrangian stochastic models of particle dispersal in the atmospheric boundary layer. *Sci Rep*. 2018 Nov 15;8(1):16843. doi: 10.1038/s41598-018-34924-4. PMID: 30442966; PMCID: PMC6237984.

Wilson, J.D., Sawford, B.L. Review of Lagrangian stochastic models for trajectories in the turbulent atmosphere. *Boundary-Layer Meteorol* 78, 191–210 (1996).<https://doi.org/10.1007/BF00122492>

Pope, S. B., & Chen, Y. L. (1990). The velocity-dissipation probability density function model for turbulent flows. *Physics of Fluids A: Fluid Dynamics*, 2(8), 1437-1449.<https://doi.org/10.1063/1.857592>

Haszpra, T., & Tel, T. (2011). Volcanic ash in the free atmosphere: A dynamical systems approach. *Journal of Physics: Conference Series*, 333, 012008.<https://doi.org/10.1088/1742-6596/333/1/012008>

Farazmand, M., & Haller, G. (2015). The Maxey–Riley equation: Existence, uniqueness and regularity of solutions. *Nonlinear Analysis: Real World Applications*, 22, 98-106.<https://doi.org/10.1016/j.nonrwa.2014.08.002>

Karten und listen seismischer Aktivitat — ZAMG. (n.d.). Zentralanstalt für Meteorologie und Geodynamik-ZAMG.<https://www.zamg.ac.at/cms/de/geophysik/erdbeben/aktuelle-erdbeben/karten-und-listen/bebendetails/austria/quakes/evid53033979>

Anthony, R. E., Ringler, A. T., Tanimoto, T., Matoza, R. S., De Angelis, S., & Wilson, D. C. (2022). Earth's upper crust Seismically excited by infrasound from the 2022 Hunga Tonga–hunga Ha'apai eruption, Tonga. *Seismological Research Letters*, 94(2A), 603-616.<https://doi.org/10.1785/0220220252>

Volcanic explosion penetrates both upper atmosphere and upper crust around the globe | U.S. geological survey. (2023, February 23). USGS.gov | Science for a changing world. <https://www.usgs.gov/news/science-snippet/volcanic-explosion-penetrates-both-upper-atmosphere-and-upper-crust-around>

Air resources laboratory - Hysplit - Hybrid single particle lagrangian integrated trajectory model. (2022, September2). Air Resource Laboratory - READY.<https://www.ready.noaa.gov/HYSPLIT.php>

Underwater fire: Studying the submarine volcanoes of Tonga. (2021, June 14). Schmidt Ocean Institute.<https://schmidtocean.org/cruise/underwater-fire-studying-submarine-volcanoes-tonga/>

IRIS: Data services: Nodes: DMC: Software downloads: PyWEED. IRIS: Data Services.<https://ds.iris.edu/ds/nodes/dmc/software/downloads/pyweed/>

Sit CESNET2. CESNET | CESNET, zájmové sdružení právnických osob.<https://www.cesnet.cz/sluzby/pripojeni/sit-cesnet2/>

Vojtech, Josef, Smotlacha, Vladimir, Havlis, Ondrej, Slapak, Martin, Altmannova, Lada, Kundrat, Jan, Bhowmick Sarbojeet, Vohnout, Rudolf, Velc, Radek, Pospisil, Petr, Cizek, Martin, Hrabina, Jan, Rerucha,

Simon, Pravdova, Lenka, Lazar, Josef, Cip, Ondrej, Kuna, Alexander, Roztocil, Jaroslav, "National Infrastructure for Dissemination of Precise Time and Coherent Ultra-stable Optical Frequency - CITAF," Proceedings of the 53rd Annual Precise Time and Time Interval Systems and Applications Meeting, Long Beach, California, January 2022, pp. 235-242.<https://doi.org/10.33012/2022.18289>

Sarbojeet Bhowmick, Josef Vojtech, and Radek Velc "Scope and application of Bi-directional EDFA for long distance optical transmissions", Proc. SPIE 11355, Micro-Structured and Specialty Optical Fibres VI, 113550P (1 April 2020);<https://doi.org/10.1117/12.2553474>

Josef Vojtech, Ondrej Havlis, Martin Slapak, Sarbojeet Bhowmick, Jan Radil, Petr Munster, Tomas Horvath, RadekVelc, Jan Kundrat, Lada Altmannova, Vladimir Smotlacha, Rudolf Vohnout, Jan Hrabina, Martin Cizek, LenkaPravdova, Simon Rerucha, Ondrej Cip, Radan Slavik, Libor Marecek, Pavel Skoda, and Michal Hazlinsky "Alternativespectral windows for photonic services distribution", Proc. SPIE 11128, Infrared Remote Sensing and InstrumentationXXVII, 1112806 (9 September 2019);<https://doi.org/10.1117/12.2529713>